An E-ELT case study

Deep, A.; Fiorentino, G.; Tolstoy, E.; Diolaiti, E.; Bellazzini, M.; Ciliegi, P.; Davies, R. I.; Conan, J. -M.

Published in:
Astronomy & astrophysics

DOI:
10.1051/0004-6361/201116603

Publication date:
2011

A&A 531, A151 (2011)
DOI: 10.1051/0004-6361/201116603

Astronomy & Astrophysics

An E-ELT case study: colour–magnitude diagrams of an old galaxy in the Virgo cluster

A. Deep[1,2], G. Fiorentino[1], E. Tolstoy[1], E. Diolaiti[3], M. Bellazzini[3], P. Ciliegi[3], R. I. Davies[4], and J.-M. Conan[5]

[1] Kapteyn Astronomical Institute, University of Groningen, PO Box 800, 9700 AV Groningen, The Netherlands
e-mail: atul.deep@esa.int; [fiorentino;etolstoy]@astro.rug.nl
[2] Leiden Observatory, Leiden University, 2300 RA Leiden, The Netherlands
[3] INAF – Osservatorio Astronomico di Bologna, via Ranzani 1, 40127 Bologna, Italy
[4] Max – Planck-Institut für Extraterrestrische Physik, Postfach 1312, 85741 Garching, Germany
[5] ONERA, 92322 Châtillon, France

Received 28 January 2011 / Accepted 16 May 2011

ABSTRACT

One of the key science goals for a diffraction limited imager on an extremely large telescope (ELT) is the resolution and accurate photometry of individual stars down to faint magnitudes in a range of environments. The aim of this study is to test the proposed capabilities of a multi-conjugate adaptive optics (MCAO) assisted imager working at the diffraction limit, in $IJHK_s$ filters, on a 42 m diameter ELT to carry out accurate stellar photometry in crowded images in an elliptical-like galaxy at the distance of the Virgo cluster. As a basis for realistic simulations we have used the phase A studies of the European-ELT project, including the MICADO imager and the MAORY MCAO module. We convolved a complex resolved stellar population with the telescope and instrument performance expectations to create realistic images. We then tested the ability of the currently available photometric packages STARFINDER and DAOPHOT to handle these simulated images. Our results show that for a one hour exposure deep colour–magnitude diagrams (photometric error, ±0.25 at $I \geq 27.2$; $H \geq 25.$ and $K_s \geq 24.6$) of old stellar populations in galaxies, at the distance of Virgo, are feasible at a maximum surface brightness, $\mu_V \sim 17$ mag/arcsec^2 (down to $M_I > -4$ and $M_H \sim M_K > -6$), and significantly deeper (photometric error, ±0.25 at $I \geq 29.3$; $H \geq 26.6$ and $K_s \geq 26.2$) for $\mu_V \sim 21$ mag/arcsec^2 (down to $M_I \geq -2$ and $M_H \sim M_K \geq -4.5$). The photometric errors, and thus also the depth of the photometry could potentially be improved with photometry packages specifically designed for an ELT MCAO point spread function. We also make a simple comparison between these simulations and what can be expected from a single conjugate adaptive optics feed to MICADO and also the NIRCAM imager on the *James Webb* space telescope.

Key words. instrumentation: adaptive optics – methods: observational – Galaxy: stellar content

1. Introduction

It is hoped that in the not too distant future extremely large telescopes (ELTs) working at their diffraction limit will be available (e.g., Gilmozzi & Spyromilio 2007; Szeto et al. 2008; Johns 2008). A telescope with a mirror diameter of ∼42 m working at the diffraction limit will have a spatial resolution of ∼10 mas in K_s filter[1] and ∼5 mas in I filter. These filters span the range of wavelengths that are planned to be covered by (relatively) wide field (>1 arcmin square) imagers making use of advanced multi-conjugate adaptive optics (MCAO). This will make a number of ground-breaking science cases possible, which can make use of the exceptional spatial resolution, and sensitivity that is possible with such a large aperture telescope (e.g., Najita et al. 2002; Hook et al. 2007; Silva et al. 2007; Kissler-Patig et al. 2009).

One of the key science cases for an ELT is the imaging and spectroscopy of individual stars in resolved stellar populations (e.g., Wyse & the Stellar Populations Working Group 2002; Olsen et al. 2003; Tolstoy et al. 2010). It is one of the three highlighted science cases for a European ELT presented by Hook et al. (2007). This science case is very broad and includes a range of targets in the Local Group (including embedded star clusters within the Milky Way) and also galaxies out to the Virgo cluster and beyond. A primary goal has long been to resolve individual stars in elliptical galaxies (e.g., Olsen et al. 2003) and to be able to unambiguously interpret their luminosities and colours in terms of a detailed star formation history and chemical evolution. The nearest predominantly old, "classical", and large elliptical galaxies are to be found in the Virgo Cluster, which contains 2000 member galaxies (Binggeli et al. 1985), with a range of morphology and luminosity, and also including ∼30 classical elliptical galaxies. There is a significantly closer example of a peculiar elliptical galaxy, Cen A (at ∼3.4 Mpc, classified as S0) but it is not representative of the class of elliptical galaxies. NGC 3379 is another closer elliptical galaxy at a distance of 10.5 Mpc (Salaris & Cassisi 1998) that is ∼0.7 mag $[(m - M)_0 \sim 30.3]$ less distant than Virgo $[(m - M)_0 \sim 31]$, but it is a single system which may not be typical (e.g., Capaccioli et al. 1991).

A science case involving resolved stellar populations is technically demanding because it requires excellent image quality (ideally at the diffraction limit) as well as optimum sensitivity. Stellar photometry requires accurate measurements over a large field of view with a substantial dynamic range in two or more broad-band filters covering as large a wavelength range as possible. The photometry of individual stars in a field of view are

[1] In this paper whenever the K filter is referred to it is always meant K_s.

then plotted in a colour–magnitude diagram (CMD) the properties of which depend upon the the star formation history and the chemical evolution of the stellar system going back to the earliest times (e.g., Aparicio & Gallart 2004; Tolstoy et al. 2009, and references therein).

Individual red giant branch (RGB) stars, of very low surface brightness ($\mu_B > 27$) regions in diffuse dwarf spheroidal galaxies in Virgo (e.g., Caldwell 2006; Durrell et al. 2007), have been photometered in long HST/ACS exposures (~10 h per filter). These CMDs contain few stars, all within one magnitude of the tip of the RGB, and with large uncertainties due to crowding. To hope to obtain deeper and more accurate photometry, and also to be able to look into the large, bright, classical elliptical galaxies in Virgo higher sensitivity and spatial resolution are required. As a minimum requirement this means detecting and accurately photometering stars in crowded images at the tip of the RGB ($M_I = -4$; $M_K \sim -6$) or stars with $I \sim 27$ and $K \sim 25$ at a signal-to-noise (S/N) ~ 4 at a surface brightness, $\mu_V \sim 19$ mag/arcsec^2. However, from the tip of the RGB alone very little information about the star formation history of a galaxy can be uniquely determined because of the well known age-metallicity degeneracy. It is important for a variety of reasons to look deeper into the stellar population, and ideally to reach the Horizontal Branch ($M_I \sim M_K \sim 0$) which means $I \sim K \sim 31$, or even the oldest Main Sequence Turnoffs ($M_I = +4$; $M_K = +3$) which means $I \sim 35$ and $K_s \sim 34$. Detecting old main sequence turnoffs is the most reliable way to accurately determine the full star formation history (e.g., Gallart et al. 2005). However, the Horizontal Branch, and to a lesser extent the shape of the RGB also provide useful constraints on the ages and metallicities of individual stars in a complex stellar population.

We can also hope to detect infra-red (IR) luminous asymptotic giant branch and carbon stars in Virgo ellipticals, which will provide an insight into the intermediate age stellar populations in these systems (e.g., Maraston et al. 2006). These stars are in many ways the ideal targets of IR surveys, but they are not representative of the over all star formation history of a galaxy (e.g., Tolstoy 2010). They are only present for intermediate age stellar populations, and even then their number is not determined by the star formation history alone.

Young stellar populations (<1 Gyr old), can also be very luminous and will be easier to study than the old populations (>1 Gyr old) for galaxies in the Virgo cluster and beyond. Very young (<10 Myr old) massive stars are much brighter than their older siblings (e.g., $M_I < -4$) but they are often buried deep in dusty molecular clouds under many magnitudes of extinction and so will clearly benefit from IR observations (e.g., Tolstoy et al. 2010, and references therein).

Here we wish to determine the feasibility of detecting and photometering old resolved stellar populations at the distance of the Virgo cluster, using technical information provided by phase A E-ELT instrument projects. The challenging demands of this goal on both sensitivity and spatial resolution, means that we require careful and detailed simulations. We simulate a stellar population over a range of surface brightness and determine how well standard photometry packages are able to cope with image crowding and how this affects the sensitivity and accuracy of the resulting CMDs. We have chosen not go into the detailed analysis of star formation histories coming from the different simulations because our main interest is in the photometric accuracy. Naturally improved photometric accuracy leads to more accurate star formation histories, and this will be quantified in future work.

Table 1. Telescope and instrument parameters for E-ELT, MICADO and MAORY.

Parameter	Value
Collecting area (m^2)	1275
Telescope throughput	0.74
AO throughput	0.80
Instrument throughput	0.60
Total throughput (including detector QE)	0.40
Read noise (e-)	5
Pixel Scale (arcsec/pixel)	0.003

Table 2. Filter characteristics in Vega magnitudes for MICADO.

Filters	I	J	H	K_s
Filter center (μm)	0.900	1.215	1.650	2.160
Filter width (μm)	0.24	0.26	0.29	0.32
Zero magnitude (ph/s/m^2/μm)	3.76×10^{10}	2.02×10^{10}	9.56×10^9	4.66×10^9
Background (mag/arcsec^2)	19.7	16.5	14.4	13.5
Background (e$^-$/s/pixel)	0.6	5.8	20.9	25.7

Using the same approach we also compare our results to those that may be expected from single conjugate adaptive optics (SCAO) and the *James Webb* space telescope (JWST) in similar filters.

2. Creating and analysing simulated images

We create realistic simulations of images of crowded stellar fields using the technical specifications provided by the European-ELT (E-ELT)[2] project based at ESO (Spyromilio et al. 2008) along with the E-ELT phase A instrument study, MICADO (Davies & Genzel 2010; Davies et al. 2010)[3] and the MCAO facility MAORY[4] (Diolaiti 2010; Foppiani et al. 2010), see Tables 1, 2 and Fig. 1. Our goal is to determine if it is possible to obtain useful CMDs of resolved stellar populations in distant galaxies, specifically elliptical-type galaxies, at the distance of the Virgo cluster (17 Mpc). This question cannot be answered using simple estimates of sensitivity and resolution because of the complex shape of the point spread function (PSF) (see Fig. 1) and the extremes of image crowding expected. Simulated images are also necessary to assess the difficulties in carrying out accurate photometry, with standard packages, given the complex PSF shape. Therefore simulations have been performed to create realistic images, varying the assumptions to understand the most important effects on the photometric accuracy and depth.

2.1. The instrument

The MICADO imager is proposed to cover a 53 arcsec square field of view at the diffraction limit of the 42 m E-ELT in I, J, H, and K_s broad-band filters, with a pixel scale of 3 milli-arcsec/pixel (3 mas/pixel). The aim is to significantly

[2] http://www.eso.org/sci/facilities/eelt/
[3] http://www.mpe.mpg.de/ir/instruments/micado/micado.php?lang=de
[4] http://www.bo.astro.it/~maory/Maory/

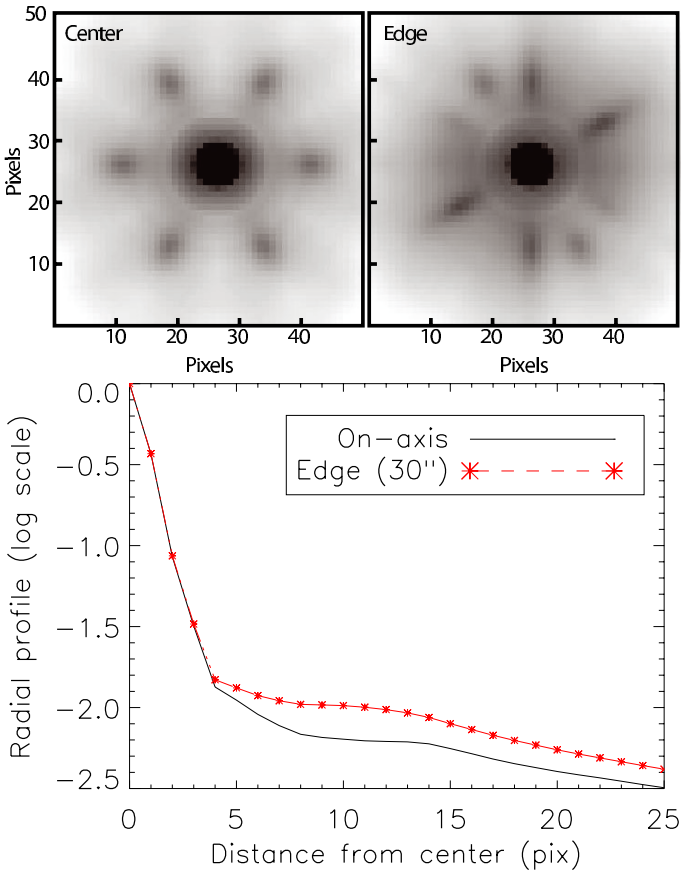

Fig. 1. We show the most challenging MCAO PSFs for the optical I filter, provided by the MAORY consortium, created assuming a seeing of 0.6 arcsec. One is at the centre, and one at a position 30 arcsec from the centre, at the edge of the field. The images are 150 mas square, thus with a pixel scale of 3 mas. The averaged radial profile compares the two PSFs over the same area as the images.

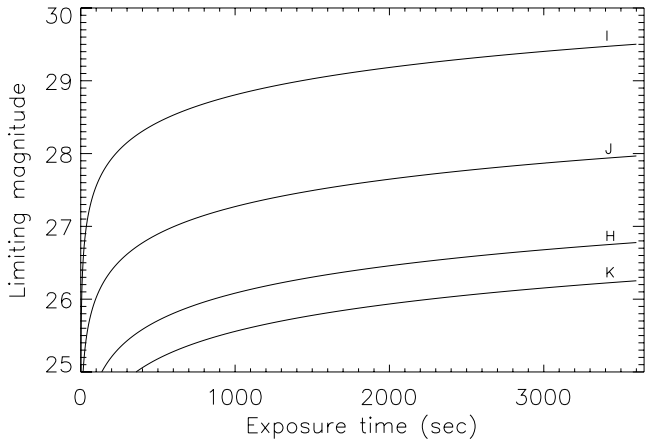

Fig. 2. Limiting magnitudes for I, J, H and K_s filters (Vega magnitudes) as a function of time for $S/N = 4$ calculated over a 50 mas aperture, assuming a seeing of 0.6 arcsec.

improve the image quality using the MAORY MCAO module, which is based upon 6 laser guide stars (LGS), for the high order sensing, in a circle 2 arcmin in diameter around the field centre. It also uses a number of natural guide stars (NGS) to measure the low order modes. This facility easily includes the MICADO field of view. The key advantage of MCAO is to increase the size of the field corrected and also the uniformity of the correction over the field. MICADO is also able to use a SCAO (single-conjugate adaptive optics) module, making use of NGS (Clénet et al. 2010), although this reduces the field of view to 45 arcsec diameter (in K_s), with a rapidly decreasing performance towards the edge of this field, especially for short wavelengths.

Photometry of resolved stellar populations to date has been predominantly carried out in optical filters (e.g., B, V and I or similar). This is certainly the preferred wavelength range to carry out accurate and deep photometry of individual stars on the Main Sequence and in cases of low interstellar extinction. This is partly because this corresponds to the peak of the luminosity distribution of the main sequence stars, and also partly because the sky background is relatively faint and stable. Excellent image quality has been obtained for deep optical exposures of resolved stellar populations at stable ground-based sites with active image correction (e.g., Paranal, Las Campanas and Mauna Kea) and most notably from space, with the Hubble Space Telescope. MICADO/MAORY on the E-ELT is likely to be most efficient at near-IR wavelengths, as this is where the Adaptive Optics (AO) performance is best. The only optical images which we can hope to obtain, with even a minimum acceptable AO performance, are through the I filter. This is also the shortest wavelength for which a MAORY PSF has been provided, and it has been provided with a number of caveats. The most important caveat is that it is at the edge of what is possible to achieve with this post-focal AO configuration combined with this telescope. The other broad band filters available are in the near-IR, namely, J, H, and K_s, and they are projected to have a much better AO performance. These filters are commonly used to study regions of heavy interstellar extinction (e.g., the Galactic Bulge, and its globular clusters), and they will remain useful to significantly extend this work.

We have carried out simulations for all the broad band filters over the full wavelength range that MICADO/MAORY will operate. Our main aim is to understand the effects of a peculiar AO PSF on the photometric results at all wavelengths, combined with the varying background level, diffraction limit, Strehl and crowding.

To predict the sensitivity of the telescope and instrument combination we used the MAORY PSFs to estimate the theoretical limiting magnitude that can be achieved with MICADO/MAORY as a function of time for $S/N = 4$ using a 50 mas diameter aperture (see Fig. 2). This value of S/N corresponds to an error of ±0.25 in magnitude [using $\sigma_{\rm error} = -2.5\log(1 + 1/(S/N))$]. These theoretical values will be compared with the results of our simulations. From Fig. 2 it can be seen that the limiting (Vega) magnitudes are $I \sim 29.5$, $J \sim 28.0$, $H \sim 26.8$ and $K_s \sim 26.2$ for an exposure time of 1 h. This is the exposure time adopted for all simulations presented here. We have also assumed cold nights with almost no thermal background to 2.32 μm. These conditions, although optimistic, are realistic and should be available for around two months every year. This assumption will have almost no effect on the I sensitivity, but a large effect on K_s, and a decreasing effect on H and J.

2.2. The point spread function

The importance of a well defined PSF for accurate stellar photometry is well documented (e.g., Stetson 1987; Schechter et al. 1993). To be able to carry out reliable photometry, which can be accurately calibrated, down to faint magnitude limits it is necessary to be able to correctly model the brighter stars and

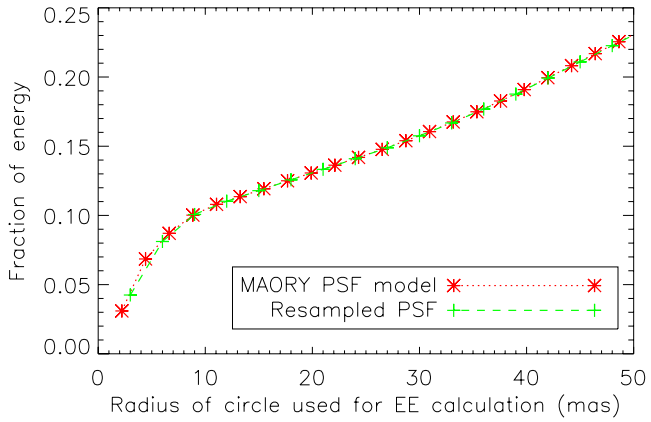

Fig. 3. For the I PSF, the EE is plotted as a function of distance from the center for the original MAORY PSF (red star symbols) and the PSF resampled to the MICADO pixel scale (green crosses).

remove them from the image to see the fainter stars below the "wings" of the brighter stars. Accurate crowded field photometry of individual stars on MCAO corrected images is challenging mostly because of the complex PSF, with a sharp central core surrounded by an extended diffuse halo (see Fig. 1), which has a strong effect on the crowding properties of stellar images. Both of these components of the PSF will vary in time and also across the field of view due to anisoplanatism. The most accurate way to assess the capabilities and the impact of an usual PSF shape over the wide field of view with an MCAO imaging system is to simulate the expected images as realistically as possible and then to analyse them using standard techniques.

Thus the most crucial aspect of making realistic simulations is to have an accurate estimate of the form and variation of the PSF. The MAORY consortium estimated the MCAO PSF modelling atmospheric and instrumental effects (Diolaiti 2010). Two PSFs in the *I* filter are shown in Fig. 1, one at the field centre and one at the edge of the field. These PSFs were last updated in March 2010, and include all major sources of error, such as the cone effect due to LGS and the NGS Wave Front Sensor errors. The I PSF is the most technically challenging, for the MCAO system, and potentially the most important for stellar population studies of the kind considered here. Figure 2 suggests that MICADO/MAORY will be able to detect significantly fainter stars in the *I* filter than in the *J*, *H* or K_s filters.

The PSFs have been calculated by sampling the diffraction limit at the Nyquist limit (approximately 2 pixels per Full Width Half Maximum). This means that all the PSFs provided have the same absolute size (512 × 512 pixels), and thus the pixel size differs with wavelength, and so all the PSFs have to be resampled to match the 3 mas pixel scale of MICADO. It can be seen that the radial average of the PSF in the lower panel of Fig. 1 is smoothed by the MICADO sampling. To obtain correct results, the resampled PSF should have a similar energy distribution to the original, especially near the centre. This is because the variation in encircled energy (EE) is very steep in the centre making it difficult to extrapolate and any error has a major effect, and photometry is typically strongly weighted by the the central pixels. After resampling, we check that the PSF energy distribution matches that of original (see Fig. 3), and as can be seen the original and the resampled PSF have almost exactly the same EE.

The two main parameters which are commonly used to evaluate AO image quality, are the strehl ratio (SR) defined as the ratio between the peak intensity of a measured point source and the ideal diffraction limited case; and the EE, defined as the fraction of the energy enclosed in a circular aperture of a given diameter about a point source. The mean values of SR and EE for the MAORY PSFs used in this work are summarised in Table 3. The EE values have been estimated for a 50 mas aperture, and are used to estimate the absolute sensitivity, shown in Fig. 2. The mean values of SR and EE in Table 3 show that MAORY achieves a high degree of uniformity and is stable over the field of view; there is only a small decrease in performance moving from the centre to the edge (~25 arcsec from the centre) of the field.

Table 3. The expected mean value for EE, for a diameter of 50 mas, and Strehl Ratio (SR) from MAORY, computed with a seeing of 0.6 arcsec.

Filters	*I*	*J*	*H*	K_s
SR(center)	0.065	0.22	0.44	0.62
SR(edge)	0.05	0.20	0.41	0.60
EE(center)	0.14	0.30	0.48	0.62
EE(edge)	0.11	0.26	0.44	0.59
EE(seeing = 0.8)	0.08	0.22	0.41	0.56
FWHM (pix)	1.76	2.03	2.33	2.60

2.3. The stellar population

A defining characteristic of an elliptical galaxy is a highly concentrated stellar population. Thus the main obstacle to deep accurate CMDs of the central regions of distant elliptical galaxies is stellar crowding, or the number of resolution elements expected per star. To properly test the capabilities of an E-ELT imaging instrument to photometer stars accurately in crowded fields it is important to create a realistic model for the stellar population. This means that the numbers, colours and magnitudes of stars are distributed as might be expected in a complex galaxy-like stellar population. The input population should include not only those stars that are expected to be detected, but also the much larger number of undetected faint stars that create unresolved background fluctuations that can significantly affect the detection limit and the accuracy of the photometry.

The primary aim of these simulations is to understand the most important effects that can limit the accuracy of stellar photometry with MICADO/MAORY. Thus we concentrate on a single stellar population, a fixed CMD, and we simply vary the total number of stars distributed in the images depending upon the surface brightness. We have chosen a stellar population that matches what might be expected for a predominantly old galaxy at the distance of the Virgo cluster (17 Mpc), see Fig. 4.

We have designed the CMD of the artificial stellar population to contain the distinct feature (see the right hand side, Fig. 4) of two narrowly separated RGBs, and this allows the eye to pick out how crowding and photometric errors effect the results. This is not meant to mimic precisely what is expected from a real stellar population, but to allow an easy assessment of the effects of increasing errors on the photometric sensitivity and fidelity. The two distinct episodes of star formation that create the CMD are an ancient population (extending from 13 Gyr ago to 8 Gyr ago) and a younger (from 7 Gyr ago to 5 Gyr ago) more metal rich population (see left panels in Fig. 4). These populations were created using IAC-STAR (Aparicio & Gallart 2004) using Teramo stellar evolution libraries (Pietrinferni et al. 2004); bolometric corrections libraries (Castelli & Cacciari 2001) and we assumed a Salpeter Initial Mass Function (IMF). All the stellar populations seen in Fig. 4 come directly from the stellar models

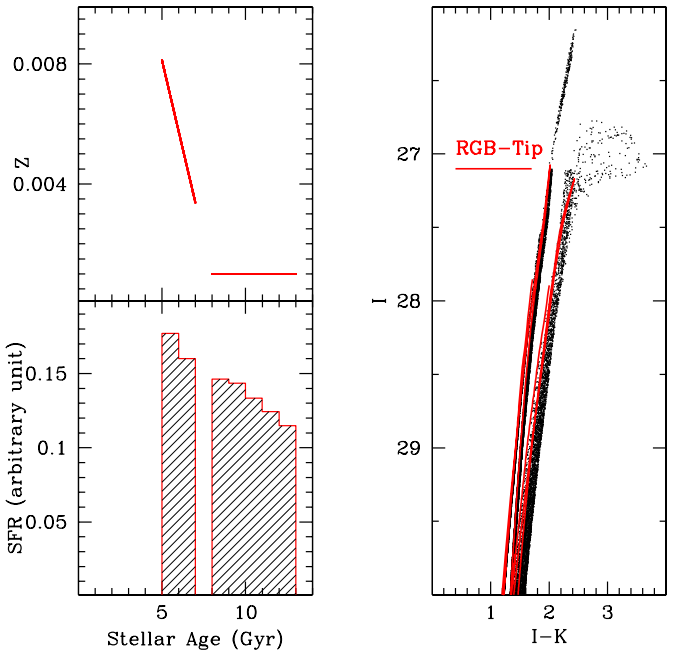

Fig. 4. Input properties of the stellar population for a predominantly old galaxy. *On the left*, the star formation rate with time is shown in the *lower panel* and the corresponding chemical evolution is shown in the *upper panel*. The resulting CMD of the galaxy, created using IAC-star (Aparicio & Gallart 2004), is shown on the right. To highlight the mean properties of the stellar populations, we have added isochrones (red solid lines) to the CMD for an old stellar population (10 Gyr) with $Z = 0.001$ and an intermediate one (6 Gyr) with $Z = 0.004$, from Pietrinferni et al. (2004).

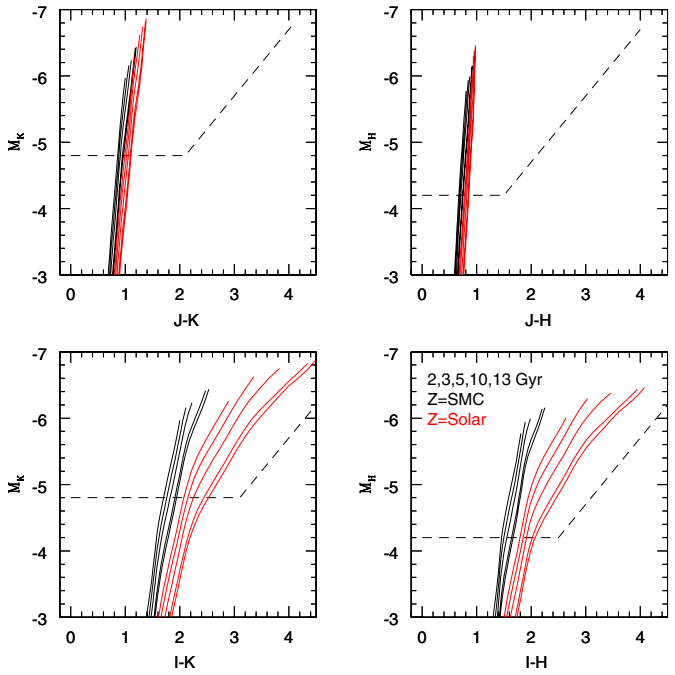

Fig. 5. Here we show a selection of 5 isochrones (from Yi et al. 2001) for SMC-like metallicity (in black) and solar metallicity (in red) for the ages 2, 3, 5, 10 and 13 Gyr old. Each panel shows a different filter combination that is possible with MICADO/MAORY. The dashed line comes from the sensitivity estimates for one hour exposures.

as implemented by IAC-star. We created a "complete" stellar population down to 0.5 $M_{\odot}$ for our chosen star formation history. For both components the models also include a bright E-AGB population above the RGB, which is predicted to be ubiquitous in elliptical galaxies. These AGB stars are easy to confuse with the RGB if the photometry is not sufficiently deep and accurate, and the distance to the galaxy is not well known. Even though this population is very luminous it can still be very sensitive to crowding effects due the substantial underlying stellar population (e.g., Stephens et al. 2003).

The stellar population we have chosen is arguably more metal poor than might be expected for a giant elliptical galaxy, but this creates a more significant photometric challenge, as the RGB is narrower than for a solar metallicity population would be for the same age range. This case will provide a limit to our ability to detect and study the metal poor component in a Virgo elliptical galaxy. Making our simulations for a more metal rich population would not change any of our results relating to the photometric accuracy. The relative number of stars for a more metal rich population will remain approximately the same, and only the colour distribution on the RGB will change. This will only affect the interpretation, and this will be investigated further in a future paper.

The differences expected on the RGB for different metallicity stars in a CMD are highlighted in Fig. 5, where it can be seen that the results of our simulations will not be significantly effected by a more metal rich population. The RGB stars will all always lie within the sensitivity limits, although the very red isochrones (the old, metal rich stars) are closer to the sensitivity limits in I, and thus their photometry may be less accurate at optical wavelengths. Thus Fig. 5 suggests that the *IR* filters are likely to be more useful to study the most metal rich stellar populations, and the optical-IR for metal poor stellar populations. For a realistic picture of the entire evolution of any large galaxy it is important that both metal rich and metal poor stellar populations are accurately surveyed and their properties quantified.

2.4. Creating the images

The stellar population described in Sect. 2.3 is combined with the instrument and telescope parameters described in Sects. 2.1 and 2.2 to create realistic images in $IJHK_s$ filters. The images have been created using the IRAF (Image Reduction and Analysis Facility) task *mkobject*. This task takes a list of stars, with magnitudes and colours from our model stellar population and, using the MAORY PSF, randomly places the required number of stars to create the desired surface brightness over the images. The parameter *zeropoint* determines the number of photons expected for a star of a given magnitude in one hour. This parameter takes into account the area of telescope, the through-put of the instrument, the Poisson photon-noise and the read-noise for the detectors (see Table 1).

We always create 0.75 arcsec square images, which correspond to 250×250 pixels. This field is a very small fraction of the full MICADO field, and it allows us not to worry about a varying PSF within a single simulation and also limits the time required to carry out the large number of simulations and the corresponding analysis. Each image is thus created with a constant PSF. This PSF will vary depending where the image fragment is presumed to lie within the full MICADO field. We actually distribute a stellar population over a still larger area (500×500 pixels), to ensure that the effect of the wings of the PSF of stars outside the primary field will not be under-estimated, as this would create an artificial "edge-effect" in the final images. Figure 6

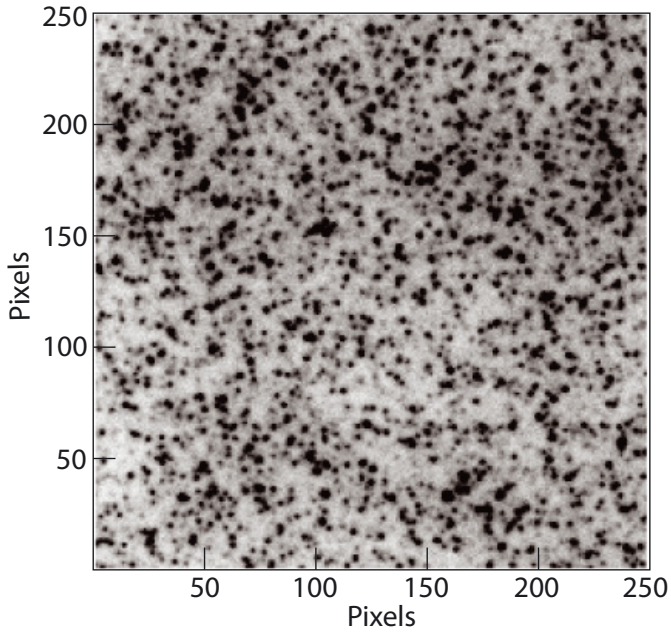

Fig. 6. A simulated MICADO/MAORY *I* filter image of a stellar field in an old galaxy at the distance of Virgo (17 Mpc). The field size is 0.75 arcsec square, with a pixel scale of 3 mas. The surface brightness of the galaxy at this position is $\mu_V \sim 19.0$ mag/arcsec^2. The image assumes an exposure time of 1 h.

shows an example of one of our simulated MICADO/MAORY images.

Our simulations are the most realistic we could make given the available information. There are however some obviously unrealistic aspects that may lead to differences with what will be delivered by a real instrument. For example, the PSF shape in our images will vary depending where the peak is placed on a pixel, and different programmes have different ways to define this. We used two different interpolation methods, one to place the PSFs and another to find and photometer them. This results in an error of ±0.03 mag on the measured flux in our photometry. This is an error that will artificially inflate the error budget of our simulations, and we have to take this into account when we assess the accuracy of our photometry.

We also always assume a single one hour exposure time for each image. This is unrealistic, since in practice very much shorter exposures will be taken and co-added. This will result in different noise properties and also a slightly broader and smoother PSF, which may serve to minimise some of the differences between real and simulated PSFs. However, it can be hoped that future instrument pipelines will be better able to handle the PSF and how it varies. This is likely to develop from an improved ability to model atmospheric variation using PSF reconstruction techniques which may lead to a better defined PSF with a well mapped out time dependence.

We are confident that our simulations realistically show the minimum that can be expected of MICADO/MAORY, from the currently available technical specifications.

2.5. Photometry

To detect and measure the magnitudes of the stars in our simulated images, we primarily used Starfinder (Diolaiti et al. 2000), a photometry package that was originally, like all others, developed to perform PSF photometry on images with a constant PSF. It was subsequently successfully adapted for the strongly distorted stars in crowded fields in SCAO images (Origlia et al. 2008). Initial attempts have also been made to deal accurately with MCAO images from MAD (Fiorentino et al. 2010). In this case the PSF does not vary as strongly as for SCAO, but the variation is much more difficult to model, in the case of MAD, because of a strongly non-uniform variation over the field of view coming from compromises made in the NGS orientation and brightness.

Starfinder works by creating a 2D image of the PSF using bright isolated stars from the observed field, without any analytic approximations. This PSF is then used as a template, which can be scaled and translated by sub-pixel offsets, to detect stars by matching their profiles against the template. The theoretical PSF can also be given directly to Starfinder, if it is known. We used the approach that is currently the most realistic to determine the PSF, as it would be for "real" observations; we extracted the PSF from the images. This extracted PSF was compared with that used to make the images and found to be in excellent agreement.

A detection threshold of 3σ above the local background is taken as the limit to which objects can be detected. First the brightest stars are identified and removed from the images, and then the images are iteratively searched to find as many faint sources as possible. This iteration is necessary to resolve crowded groups to separations comparable to the limits allowed by the width of the PSF.

2.6. Surface brightness and crowding

The accuracy and the magnitude limit of the photometry from MICADO/MAORY images towards the high surface brightness centres of elliptical-like galaxies in Virgo will be strongly affected by the extreme crowding of unresolved stars. This crowding is partly caused by the large low surface brightness halos surrounding the core of each PSF, but also simply due to the extremely dense stellar population and the fact that we can only resolve the brightest stars. The higher the surface brightness the more densely packed will be the stellar population and the higher will be the unresolved background. This effect is well known, and has been the subject of much study over the years, starting in radio astronomy (e.g., Scheuer 1957; Condon 1974) and more recently also in optical and IR studies of crowded stellar populations (e.g., Gallart et al. 1996; Renzini 1998; Olsen et al. 2003; Stephens et al. 2003).

The extended halos of MCAO PSFs are hard to model accurately in current photometry packages, and this makes crowding effects particularly acute. A poorly subtracted background limits the detection of fainter stars lying below the extended PSF wings of brighter stars. Here we quantify how the surface brightness of an image relates to magnitude and crowding limits to detect and photometer individual stars. The complex PSF, as well as the significant underlying stellar population, means that the photometric accuracy is not a simple relation between the number of stars and the number of pixels, although this does, of course, provide a hard limit. It is important to verify the difference between the theoretical magnitude limits and what can be achieved with on the images themselves.

In all cases most of the stars in our simulated images lie below the detection threshold. We found that stars which are more than 2 mag fainter than the detection threshold will only contribute a uniform flux to the background level, and so they were added as such. The rest of the stars were added individually. The undetected stars are seen as fluctuations just below the detection threshold. These have a significant effect on the

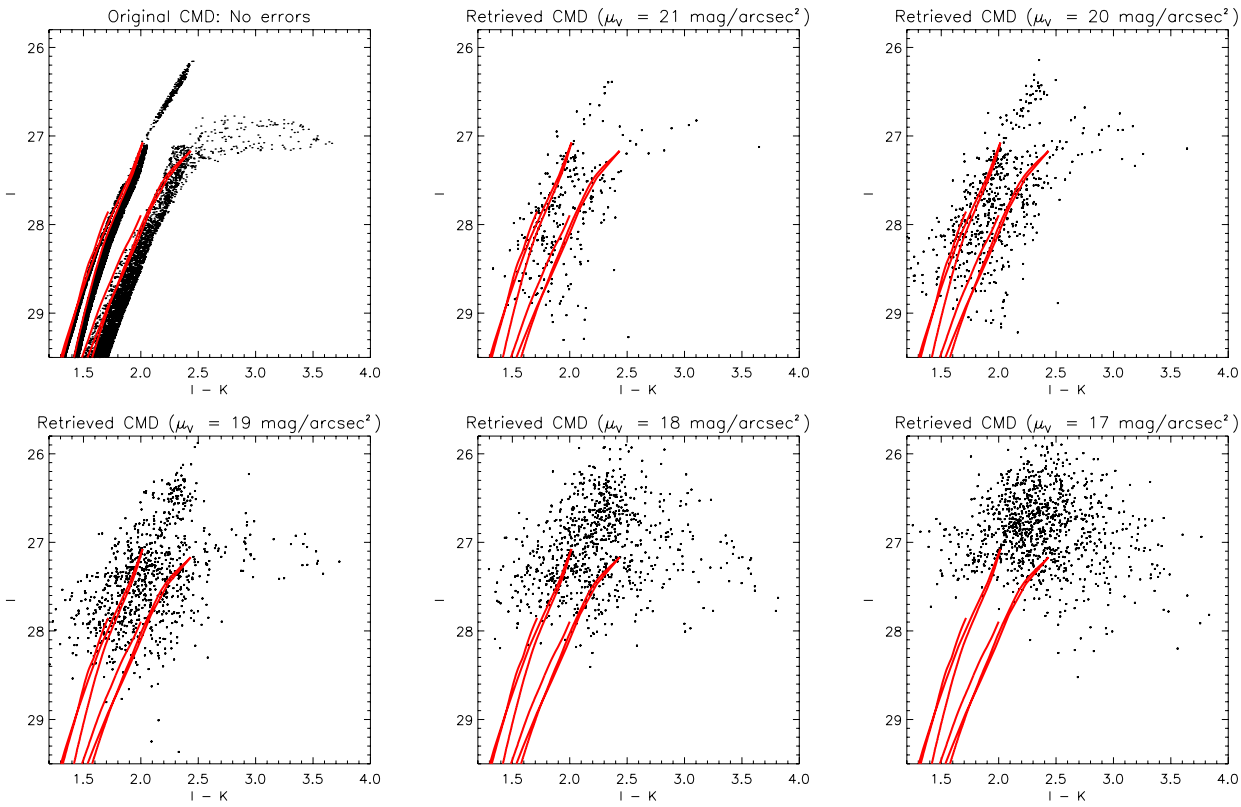

Fig. 7. The $(I, I{-}K)$ CMDs obtained from Starfinder photometry of simulated MICADO/MAORY images for 5 different surface brightness (μ_V) levels. The *top left* hand corner is the original input CMD, without any errors. Included on each panel are the isochrones which represent the mean of the properties of each distinct stellar population, namely $Z = 0.001$; 10 Gyr old and $Z = 0.004$; 6 Gyr old. The highest surface brightness (μ_V = 17 mag/arcsec^2) is equivalent to a distance of ∼5 arcsec from the centre of a typical elliptical galaxy in Virgo (e.g., NGC 4472), whereas the lowest (μ_V = 21 mag/arcsec^2) is at a distance of ∼75 arcsec from the centre.

photometric accuracy of the resolved stellar population, as they create a highly variable background.

To study crowding effects the density of the stellar population is varied from 20 000 to 500 000 stars (going 2 mag below the detection threshold in each filter) per 0.75 arcsec square image. In fact, for this particular stellar population, at this distance, the background of unresolved stars increases faster, with surface brightness, than the crowding limit of detected stars. The number of stars put into an image correspond to a surface brightness (μ_V), and we have chosen to test five different values: μ_V = 21, 20, 19, 18 and 17 mag/arcsec^2. The maximum and minimum were chosen such that the 250 × 250 pixel images always contained a statistically useful number of stars which could be accurately photometered. In the case of the lowest surface brightness (μ_V = 21) this relates directly to the low stellar density, but for the bright limit (μ_V = 17), it is the high flux in the unresolved background that limits the number of stars that can be accurately photometered.

3. The results: colour–magnitude diagrams

From the simulated images in the four broad-band filters (I, J, H, and K_s) which have been photometered with Starfinder at five different surface brightness levels we obtained a variety of CMDs. For example the results for (I, $I{-}K$), which cover the longest colour baseline, are shown in Fig. 7. The effect of increasing crowding on photometric depth and accuracy can clearly be seen. We have chosen not to carry out a detailed star formation history analysis on the simulations, but it can clearly be seen that the two distinct populations on the RGB merge more and more into an indistinct blob, and the faint stars disappear as the surface brightness and hence the crowding increases. The two distinct input stellar populations can barely be distinguished in the highest surface brightness CMDs. This is mostly due to the increasing background due to ever larger numbers of unresolved stars, but also partly due to the increased crowding of the detected stars. Severe crowding can make it difficult to accurately measure the magnitudes of even the brightest stars.

To make the most efficient use of precious telescope time we should determine what is the best combination of the available filters to obtain the most sensitive and accurate CMDs that can be interpreted with the least ambiguity. It would seem that the combination $(I, I{-}K)$ should lead to the most detailed CMD, as can be seen from a set of isochrones (e.g., Fig. 5), and comparing them with the sensitivity limits (Fig. 2). This is because the colour is more spread out when the I filter is included, and the colour range of the isochrones is broader, which makes it easier to separate populations of different ages. However, this has to be tested with our simulations, because the AO performance in the I filter is very poor. The filter combination with the best AO correction is $(K, J{-}K)$, and there are examples in the literature where the optical-IR CMDs contain the same details as IR CMDs alone (e.g., Sollima et al. 2004, for Omega Cen) despite the compression of the colour scale. Thus to test the difference between $J{-}K$ and $I{-}K$ CMDs we have colour coded the two distinct stellar populations in our simulations and compared the CMDs at the same surface brightness (19 mag/arcsec^2), as shown in Fig. 8. It can be seen that the "observed" CMD is better

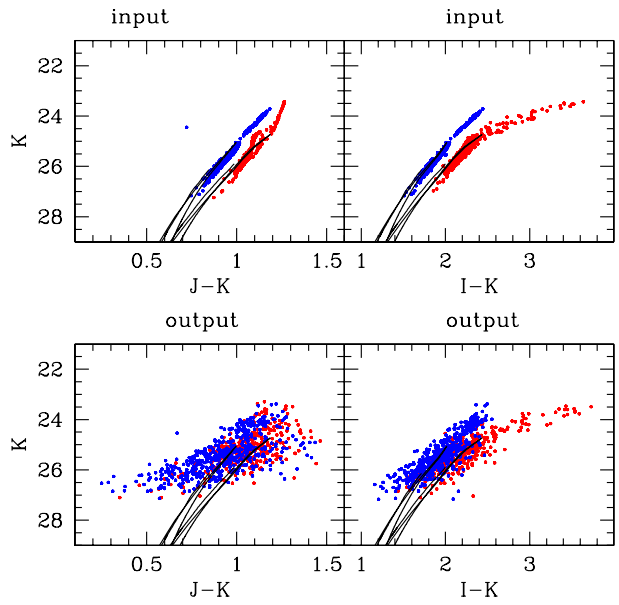

Fig. 8. Here we show the stellar population that is the input to the simulated images (*upper panels*) and the output photometry measured (*lower panels*), in $(K, J-K)$ and $(K, I-K)$, assuming a surface brightness, $\mu_V = 19$ mag/arcsec^2, for the stellar population defined in Fig. 4. The two distinct star formation episodes are colour coded, so that the impact of the different filter choices can be better judged.

defined in $(K, I-K)$, specifically the upper parts of the two RGB branches and the AGB stars can be more clearly distinguished. This is mostly due to the small colour difference between these two populations in $J-K$.

It is perhaps surprising that $I-K$ is a better combination than $J-K$, as the AO correction in the I band is very poor. However for the stellar population we have chosen the poor AO correction in I is compensated by the low sky background (see Table 2). This will not be true for very red stars, such as carbon stars and metal rich AGB stars which are intrinsically brighter in the IR. It will also not be true if there is severe reddening, which is where only IR photometry will be able to penetrate the dust and produce accurate and sensitive CMDs. In our simulations we always assume that reddening is very low.

In summary, Fig. 8 shows that although $(K, I-K)$ is preferable; with carefully modelling $(K, J-K)$ can still provide valuable information about the colour and the spread of the RGB and AGB populations. We concentrate our effort for the rest of the paper on the properties of the I and K_s filters as these provide the deepest and most accurate CMDs for the stellar population we have chosen.

The two most important effects that dominate our ability to carry out an accurate scientific analysis of deep images of resolved stellar populations are the photometric errors and the completeness of the detections, and of course they are both intricately dependent on each other. Errors from photometry determine how accurately we can distinguish between different stellar evolution models, and hence how accurately we can determine the ages and metallicities of the stars in a complex stellar population. The completeness, or fraction of the stars of a given magnitude that are detected, is important because stellar evolution models make predictions about the relative numbers of stars of different magnitudes. This means it is important to know the fraction of a population that is detected to be able to distinguish evolutionary effects from measurement bias.

3.1. Photometric errors

Our simulations allow a straight forward determination of how well the photometry is carried out because we know a priori the properties of the input stellar population. This means that we can accurately quantify the photometric errors for a range of different conditions by simply matching the input and output catalogues. We compute the rms measurement error for each magnitude bin and these values are plotted for different μ_V in Fig. 9. These rms values are prone to statistical errors due to the finite numbers of stars in each bin. Bins that contain fewer stars will have a larger rms error than the more populated bins. To mitigate this effect we put 50 test stars in every bin and based our error estimates solely on these stars.

In Fig. 9, as expected, the photometric errors become steadily larger towards fainter magnitudes in all filters and for all surface brightness values. The effect of increasing surface brightness is to make the photometric error at a given magnitude larger. It can be seen that for a surface brightness, $\mu_V = 19$ mag/arcsec^2, which implies a distance of ~25 arcsec from the center of a typical giant elliptical galaxy, like NGC 4472, for stars of magnitude $I \sim 28.2$, $J \sim 27.2$, $H \sim 25.7$ and $K_s \sim 25.4$ we can achieve a photometric accuracy of ±0.25 mag. If we want to probe closer to the centre of a giant elliptical galaxy, say within 5 arcsec ($\mu_V = 17$ mag/arcsec^2), we can do that for stars with magnitudes $I \sim 27.2$, $J \sim 26.2$, $H \sim 25.0$ and $K_s \sim 24.6$ or brighter, with the same error. It is reassuring to see that for the least crowded images the limiting magnitude and error in Fig. 9 corresponds well to the theoretical predictions in Fig. 2.

It can also be seen in Fig. 9 that even at the brightest magnitudes the photometric error is always larger than would be typical for HST or high quality (non-AO) ground based studies. These are certainly inflated by the errors due to the different PSF interpolation methods (see Sect. 2.4), but also the photometry packages are not optimised for the extremely extended and irregular MCAO PSF (see Fig. 1). Photometry of MCAO images is clearly an area which requires further development, independent of instrument hardware.

From Fig. 9 we can see that, as was predicted in Fig. 2, the I magnitude has a much fainter limiting magnitude than J, H or K_s. This is because of the lower sky background in I. This would suggest that the limiting factor in obtaining a deep CMD with MICADO/MAORY is the *IR* magnitude. However, the fact that the same photometric error is obtained at $I = 28.2$ and $K_s = 25.4$ does not necessarily mean that I is always better than K_s. This depends on the colour of the star being observed. This difference is actually optimal for a star with $I-K \leq 2.8$. If the star is any redder than this ($I-K > 2.8$) then the sensitivity of the I filter begins to be the limiting factor. In Fig. 10, we show the contribution of the errors in all filters as a function of the K magnitude. It can be seen that at the limit of the K_s sensitivity, the I error is actually dominating the uncertainty in the $I-K$ colour. This is because I has to be significantly more sensitive than K_s to match the accuracy of photometry for the same RGB star.

3.2. Completeness

A fraction of the stars in an image are always, for a variety of reasons, not detected. This is called the completeness fraction, and it needs to be determined to be able to correctly interpret

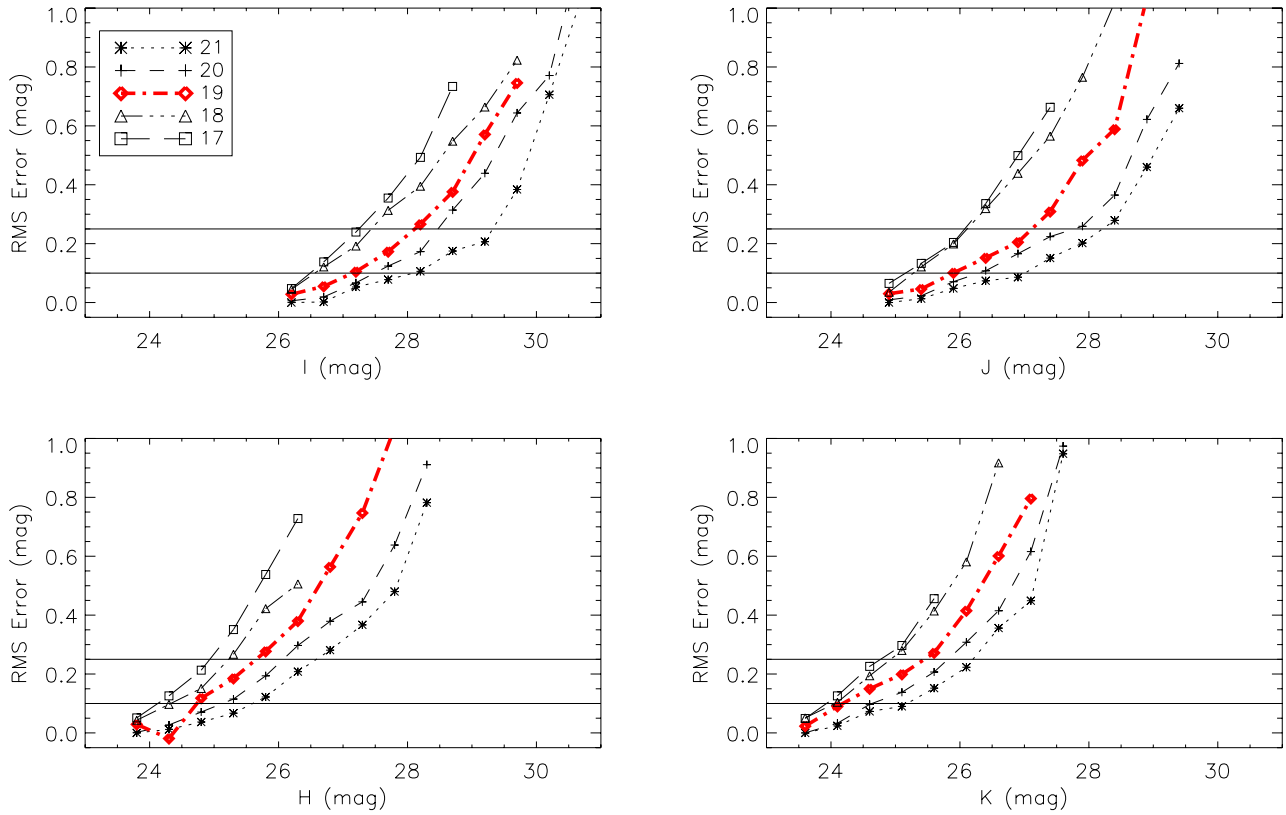

Fig. 9. The photometric errors for the simulated MICADO/MAORY images in I, J, H, and K_s filters. The results are given for 5 different surface brightnesses (μ_V), corresponding to the CMDs in Fig. 7. Highlighted (in red) is the case for a surface brightness, $\mu_V = 19$ mag/arcsec^2, in each filter. This corresponds to a distance of ∼25 arcsec from the centre of a typical giant elliptical galaxy, like NGC 4472.

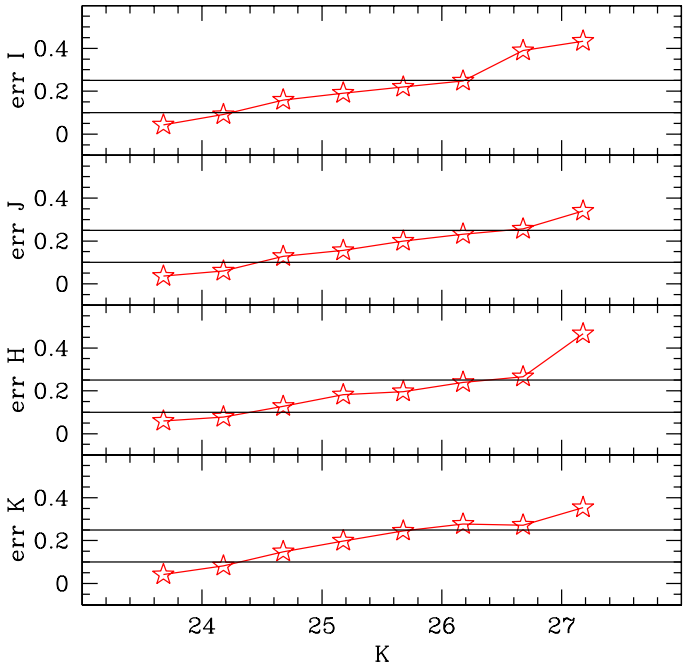

Fig. 10. Here we show for the I, J, H, K_s filters, the errors on the photometry, as a function of K_s magnitude. This shows the limiting filter on the photometric accuracy of the colour in a CMD as a function of K_s magnitude.

an observed CMD. As with the photometric errors, this effect can easily be quantified in our simulated images, by comparing input and output catalogues. For "real" observations, this is a much more laborious process, that requires artificial star tests to determine the retrieval rate for different magnitude ranges. The completeness results are shown in Fig. 11, where it can be seen that the bright stars are almost always retrieved even at high surface brightness. The completeness declines for fainter stars at a rate that accelerates with increasing surface brightness. The completeness fraction is comparable in I and J, and both have a higher completeness at fainter magnitudes than H and K_s. However, as for the photometric errors the appropriate comparison is the I and K_s completeness with an offset in magnitude related to the colour on the RGB at that magnitude.

We also note that the number of "false" detections, that is stars which are incorrectly identified in the images, is higher in the I images, than in the K_s images. This is most likely because I has a very poor AO correction compared to K_s (see Table 3), and so the I PSF is much less peaked and therefore it is easier to find spurious sources.

3.3. Natural seeing

The natural seeing conditions in the atmosphere above the telescope/instrument have an effect on the properties of the PSF on the image, even after AO correction. The MAORY consortium has produced PSFs for a natural seeing of both 0.6 and 0.8 arcsec. As expected, even though it is a small effect, I images are more affected by seeing conditions than K_s. For 0.6 arcsec seeing, a photometric accuracy of 0.25 is achieved for an $I \sim 28.1$ star. With 0.8 arcsec seeing, the same accuracy will be achieved only for stars with $I \sim 27.7$ mag. There is no effect at

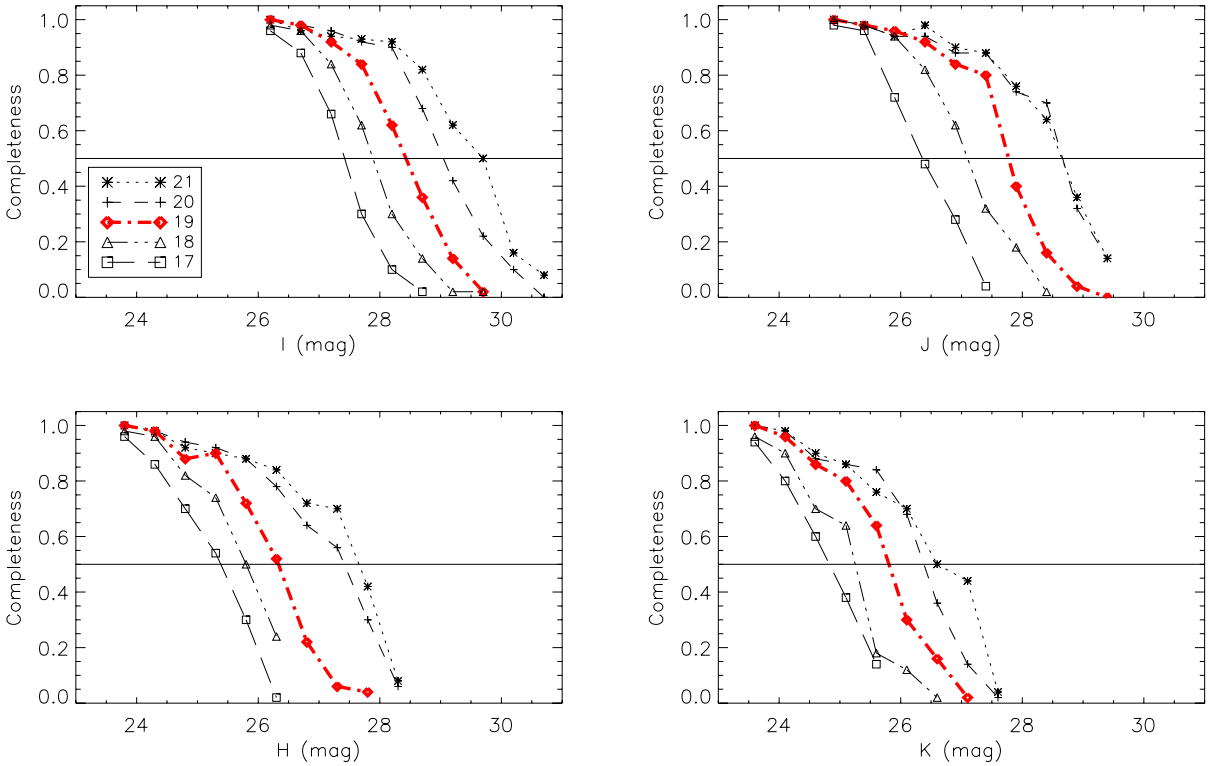

Fig. 11. Completeness fractions, which are defined as the fraction of input stars retrieved in the output catalogues at given magnitudes, for MICADO/MAORY images in I, J, H, and K_s filters. The results are given for five different surface brightness (μ_V) Highlighted (in red) is the case for a surface brightness, $\mu_V = 19$ mag/arcsec^2, in each filter, which implies a distance of around 25 arcsec from the center of a typical giant elliptical galaxy, like NGC 4472.

bright magnitudes, and especially in K_s the effect at all magnitudes is small.

3.4. The effect of a different stellar population

If we look at a younger galaxy, still forming stars, or a galaxy closer by (or further away) the main effect is going to be, for the same surface brightness, a different level of background fluctuations. This is because the characteristics of the underlying stellar population, that which is below the detection level, will change. For example, nearby galaxies will be more fully resolved into stars than distant galaxies for the same observing time. This means that the effects of an unresolved stellar background will become less. The sensitivity and crowding limits determined for a distant galaxy will be an over estimate for a nearby galaxy. Large numbers of very young bright stars will also have an effect on the photometric sensitivity and crowding, because their PSF halos will increase the background and strongly affect the fainter stars. This effect is stronger in I filter than in the IR filters, which is due to the poor AO correction in I.

In Fig. 12 we compare photometric accuracies in I achieved at the same surface brightness for a nearby galaxy (uniform background) and more distant (fluctuating background) stellar populations. As can be seen the presence of different background fluctuations can have a significant impact on photometric accuracy at high surface brightness.

When very nearby galaxies are observed it will be important to take wide field images to sample the variation in a galaxy (e.g., a spiral galaxy) or to get sufficient stars to properly populate a CMD (e.g., Local Group galaxies).

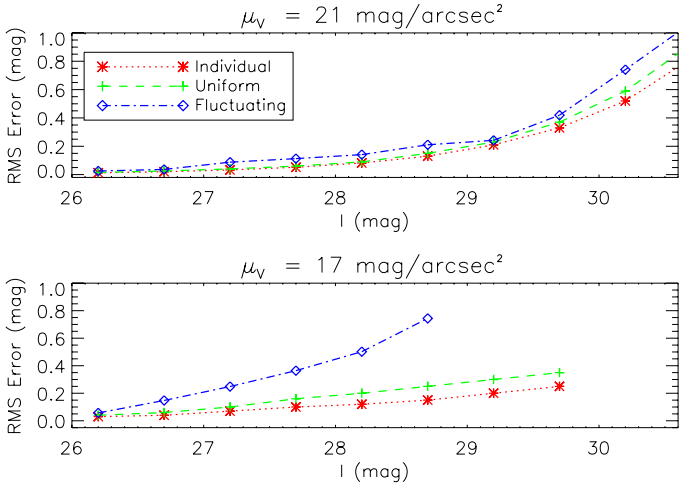

Fig. 12. The effect of the type of background fluctuations on photometric accuracy, for two different surface brightness, $\mu_V = 21$ (*upper panel*) and $\mu_V = 17$ (*lower panel*). In each panel three cases are considered for the same stars detected: individually, the theoretical value; on a uniform background; and those detected on a fluctuating background. They are labeled, respectively, individual (red); uniform brightness (green); fluctuations (blue).

3.5. Comparison with DAOPHOT/ALLSTAR photometry

We made a comparison between the photometry obtained with Starfinder and the commonly used DAOPHOT/ALLSTAR (Stetson 1987), which uses a different approach to define and map the PSF. DAOPHOT models the PSF using the sum of analytic bi-variate symmetrical functions combined with an

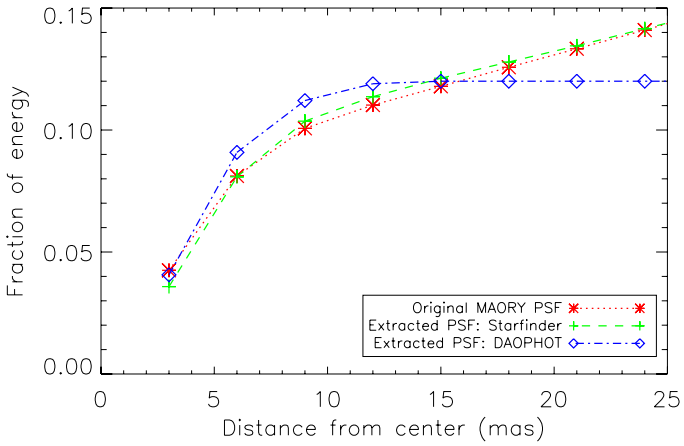

Fig. 13. A comparison between the encircled energy as a function of distance from centre of the field in the I filter, for the original MAORY PSF (red); the PSF extracted by Starfinder (green); and that extracted by DAOPHOT (blue).

empirical look-up table that provides corrections to the final function. This PSF is determined on the observed images using the average profile of numerous stars over the field pf view. This approach offers flexibility in modelling complex PSFs, even when AO is used. It has been successfully tested on MCAO images from MAD (e.g., Fiorentino et al. 2010) with a strongly varying PSF.

For the PSF determination in DAOPHOT we selected ∼100 isolated stars in a low surface brightness image to estimate the PSF. We then left DAOPHOT free to choose the best fitting form for the PSF. A comparison of the EE distribution for the DAOPHOT PSF and both the theoretical MAORY PSF and that extracted from the images by Starfinder is shown in Fig. 13. The Starfinder PSF is closer to the shape of the input PSF. This is because Starfinder is extracting the PSF directly from the image, whereas DAOPHOT makes a model. However in both cases the final integrated fluxes are very similar.

In Fig. 14 we show the comparison of the photometry from DAOPHOT and Starfinder for both completeness and photometric accuracy at a surface brightness, $\mu_V = 20$ mag/arsec^2. We can see that despite the differing accuracy in modelling the PSF, the photometry obtained from DAOPHOT is similar in terms of both accuracy and completeness, to that obtained from Starfinder for both I and K_s photometry. However, given that Starfinder more accurately reproduces the PSF shape, it is likely to be more accurate in more crowded stellar fields.

There is clearly room for improvement in existing photometric packages to properly account for a complex MCAO PSF, and this should lead to more accurate photometry especially at the fainter magnitudes. This is unlikely to significantly affect the absolute detection limits, which match the theoretical predictions, but it should make the errors smaller for fainter magnitudes which will allow a significant improvement in our ability to interpret the CMDs.

3.6. Single conjugate adaptive optics

A simpler option for AO corrections is single-conjugate adaptive optics. This uses only one guide star to measure the wavefront phase. In this case, the corrected field of view is limited by the position of the science target with respect to the guide star, and to some degree also by the properties of the guide star.

This option is being considered for (early) use with MICADO, and so we also consider the performance that may expected for our science case. We have performed simulations for the same stellar population used through out this paper (see Fig. 4), but using a PSF for SCAO mode with a NGS. The PSFs were calculated using the analytic code PAOLA (Jolissaint et al. 2006). This exercise has been carried out in both I and K_s filters to compare the impact of anisoplanatism on the photometric accuracy over the range of available wavelengths.

The main difference for SCAO images, compared to MCAO, is the presence of anisoplanatism, which is a strong, colour dependent, variation of the PSF with distance from the NGS. Using a version of Starfinder that has been adapted for SCAO images (Origlia et al. 2008), we find that the photometry becomes increasingly inaccurate and less sensitive with increasing distance from the guide star (see Fig. 15), especially in I filter. This is largely because the stars become significantly more elongated, and spread out over more pixels which reduces the sensitivity and the spatial resolution. The degradation in the CMD quality and depth as we go off-axis, seen in Fig. 15, is mainly due to increasing errors in I photometry. The photometric accuracies remain relatively small for K_s band even 15 arcsec from the guide star. This suggests that $J-K$ is a better combination for making accurate CMDs with SCAO, and also for making maximum use of the available field of view.

4. Comparison with other facilities

In order to assess how realistic the our simulations may be, we make a broad comparison with results from MAD (multi conjugate adaptive optics demonstrator), an MCAO instrument that was tested on the VLT in 2007 and 2008. This comparison is necessarily qualitative, as MAD is a very different MCAO system to MICADO/MAORY. MAD relies solely on NGS, and also the VLT is a much smaller telescope than the E-ELT will be.

We also make a comparison with a future space based imager, NIRCam (near-IR Camera), on JWST a 6.5 m IR optimised space telescope which is scheduled for launch in ∼2018. This is arguably the closest competition for ELT imaging with MICADO/MAORY.

4.1. MAD on the VLT

The only MCAO system, which has been thoroughly tested on the sky, is MAD[5]. This proto-type instrument was built for the VLT to prove the concept of MCAO with NGS (see Marchetti et al. 2006, for details). It had three optical Shack-Hartmann wavefront sensors for three NGS with limiting magnitudes of $V \sim 13$ mag. The NGS were ideally to be located on the vertexes of an equilateral triangle within a field of 2 arcmin diameter. The MAD detector had a pixel scale of 0.028 arcsec per pixel over a ∼1 arcmin square field. Several studies of Galactic stellar fields have been published from this successful experiment (e.g., Momany et al. 2008; Moretti et al. 2009; Bono et al. 2009; Ferraro et al. 2009; Sana et al. 2010). The Large Magellanic Cloud (LMC) was the most complex and crowded extra-galactic stellar population studied with MAD (e.g., Campbell et al. 2010; Fiorentino et al. 2010). All these studies showed the relative ease of use of MAD for accurate and deep IR photometry of point

[5] See http://www.eso.org/sci/facilities/develop/ao/sys/mad.html for details.

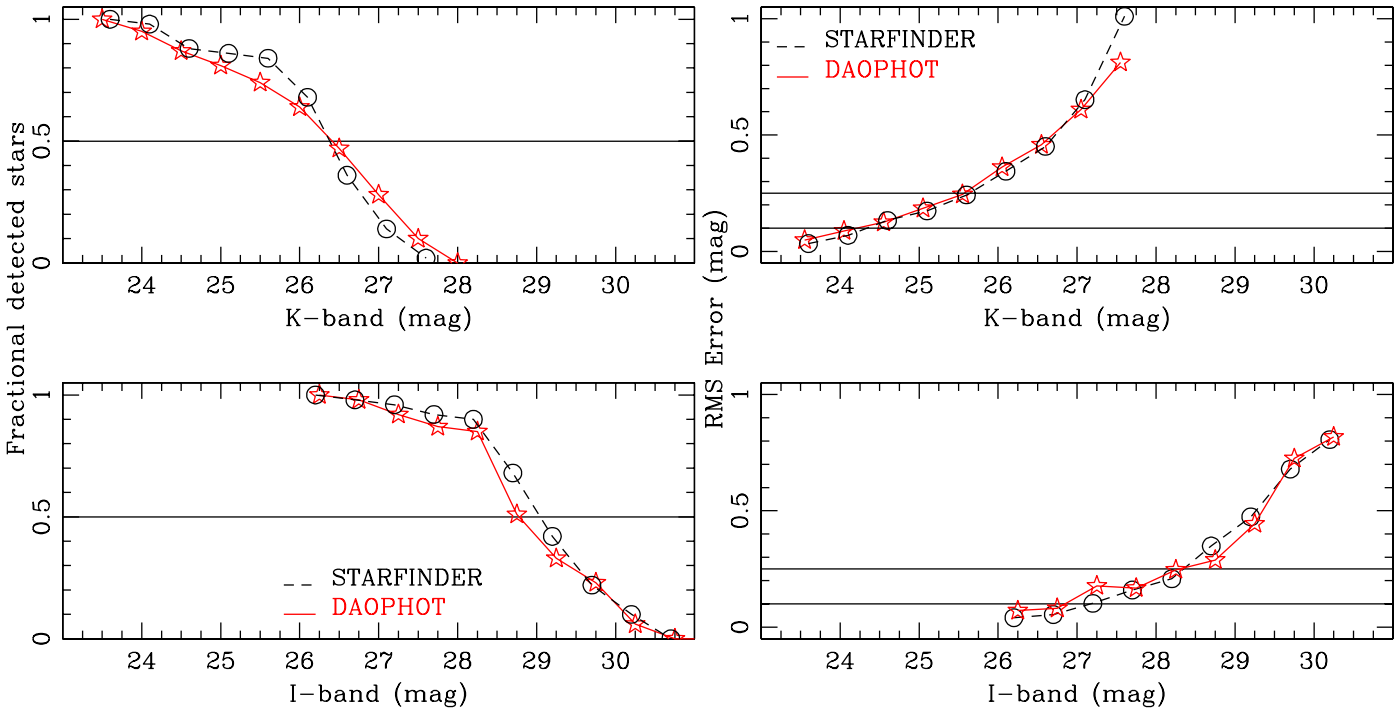

Fig. 14. The comparison between the I and K_s-band completeness (*left*) and photometric errors (*right*) from Starfinder (black) and DAOPHOT/ALLSTAR (red) for MICADO/MAORY images at μ_V = 20 mag/arcsec^2.

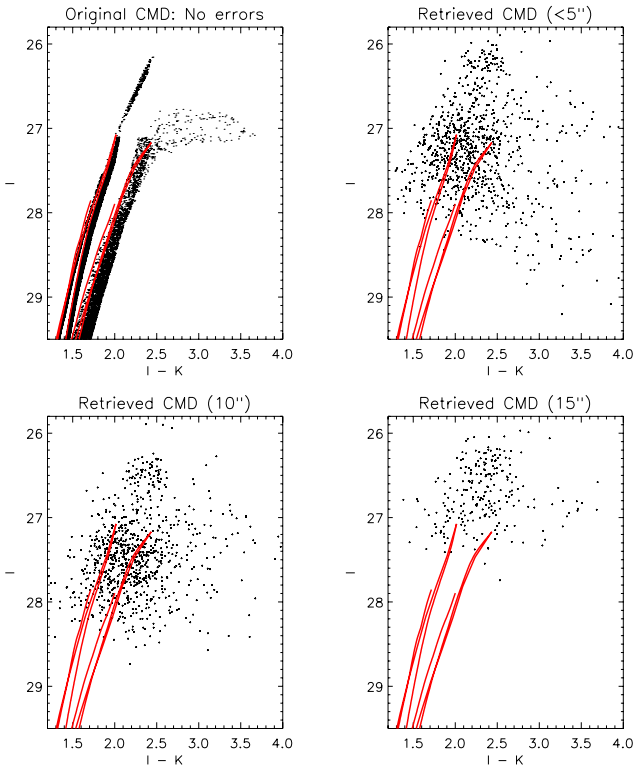

Fig. 15. Here we show the effect of anisoplanatism for 0.75 arcsec square MICADO/SCAO images, with a surface brightness, μ_V = 19 mag/arcsec^2 for a range of distances off-axis from the single guide star. The input CMD, and the isochrones are the same as in Fig. 7.

sources in crowded fields. The main limitation has been to find suitable asterisms around interesting science targets.

The difficulties in directly comparing MAD with MICADO/MAORY lie in the large variation in performance that result from relying on a suitable configuration of three NGS. The important technical achievement of MAD has been to reach the diffraction limit of the VLT in K_s band, 0.07 arcsec (e.g., Falomo et al. 2009). In H band the performance has also been very good, regularly achieving images within a factor two of the diffraction limit (0.05 arcsec). For all the projects it was found that even if the observing conditions were rarely optimum the correction achieved with MAD was always an improvement over seeing-limited imaging and also over SCAO imaging (Fiorentino et al. 2010).

It is also encouraging that standard the photometry package DAOPHOT worked very well on MAD images, and was also able to trace the PSF variation across the field. The MAD photometry combined with optical photometry from HST showed that the techniques applied so far tointerpret the star formation history of a galaxy, observed in V and I, can be confidently applied to the IJK images that we are likely to obtain with MICADO/MAORY on an E-ELT (e.g., Fiorentino et al. 2010).

MICADO/MAORY will of course be a much more efficient system, first and foremost because the LGS will provide a more stable AO correction, but also because many of the problems with MAD are related to the fact that it was a test facility optimised only in K_s. MAD has proven that MCAO works very well, and consistently with theoretical expectations. This gives us confidence that our simulations are realistic.

4.2. NIRCam on JWST

A potential competitor for MICADO/MAORY imaging will be NIRCAM[6] on JWST (Rieke et al. 2005). A telescope in space always has the huge advantages of image stability and low sky background compared to terrestrial facilities. NIRCam

[6] http://ircamera.as.arizona.edu/nircam/

is a designed to work over the 0.6 to 5 micron wavelength range. It will cover a larger field of view than MICADO (2.2 arcmin square). However it will have a much larger pixel size, of 31.7 mas. NIRCam is predicted to have similar sensitivity in $IJHK_s$ filters to MICADO/MAORY, although the filters of JWST/NIRCam are somewhat different to those of MICADO/MAORY, compare Tables 2 and 4. The similar sensitivities are because the small collecting area of JWST (6.5 m diameter) is compensated for by the extremely low background flux in space (see Table 4). However, the JWST primary mirror size means that the diffraction limit is considerably larger than an E-ELT, and the pixel size reflects this. This means that MICADO/MAORY will always be able to resolve individual stars at significantly higher surface brightness than NIRCam.

We simulated JWST/NIRCam images for the I and K_s filters in the same way as for MICADO/MAORY. We used the technical specifications found on the JWST/NIRCam public webpages[7], see Table 4. The PSFs were made using the JWPSF software tool (Cox & Hodge 2006), which provides PSFs that are oversampled by a factor of 4, and they had to be resampled to match the pixel scale of NIRCam. We created images with the same 1 h integration time used for all the E-ELT simulations. We also carried out the photometry of the images using Starfinder to make CMDs (see Fig. 16). It is obvious, that the surface brightness level that we can photometer with NIRCAM is much fainter than MICADO/MAORY for the same stellar population at the same distance. This is due to the order of magnitude difference in the diffraction limit between the two instruments.

Comparing MICADO/MAORY and JWST/NIRCam photometry is not straight forward because the highest surface brightness simulations for which we could carry out photometry with JWST/NIRCam images is $\mu_V = 22.9$ mag/arcsec^2, which is lower than the lowest surface brightness considered for MICADO/MAORY (21 mag/arcsec^2). The surface brightness limit of NIRCAM, with severe crowding, is completely uncrowded in MICADO/MAORY images. At $\mu_V = 22.9$ mag/arcsec^2 in the I filter with NIRCam, we find a photometric accuracy of ±0.25 mag is reached with a star of apparent magnitude $I = 27.1$, and for MICADO/MAORY, this limit is $I = 29.3$, see Fig. 17. Thus, for the same surface brightness, MICADO/MAORY will be able to detect stars >2 mag deeper in I band than NIRCam. The situation is less dramatic for the K_s filter, where for the same surface brightness, $K = 26.2$ is the limit for MICADO/MAORY and $K_s = 25.6$ for NIRCam, see Fig. 17. The difference is only ~0.5 mag deeper for MICADO/MAORY. This is because of the dramatically lower background for K_s in space.

This comparison is less clear-cut if uncrowded images for both instruments are compared. That is at a surface brightness of $\mu_V = 25.4$ mag/arcsec^2 for NIRCam, $I = 28.8$ is reached with a photometric accuracy of ±0.25mag, which is within 0.5 mag of the MICADO/MAORY uncrowded limit for the same photometric error. For the same, uncrowded surface brightness in K_s, the NIRCam limit is $K_s = 27.25$, which is more than ~0.5 mag deeper than the MICADO/MAORY uncrowded limit. However these uncrowded JWST/NIRCam images will only be possible for very low surface brightness systems (like dwarf irregular galaxies) and the distant outskirts of massive elliptical and Spiral galaxies at the distance of Virgo.

The different surface brightness regions that can be efficiently photometered by E-ELT (with MICADO/MAORY) and JWST (with NIRCAM) in I and K_s filters are highlighted in Fig. 18, which shows that only MICADO/MAORY can carry out photometry for surface brightness, $\mu_V < 23$ mag/arcsec^2, with a reasonable photometric accuracy (±0.25) and sensitivity. The sensitivities for both E-ELT and JWST fall off sharply at the limit of the image crowding mostly due to the increase in the background caused by increasing numbers of unresolved star below the detection limit for increasing surface brightness.

Of course for NIRCam the image is quality is likely to be much more stable than for MICADO/MAORY, however the sensitivities and completeness measures of crowded NIRCam images show that the major effect is the unresolved background flux which only a higher spatial resolution can resolve out.

[7] http://ircamera.as.arizona.edu/nircam/features.html

Table 4. Filter characteristics in Vega magnitudes for NIRCam on JWST.

Filters	I	J	H	K_s
Filter centre (μm)	0.900	1.15	1.50	2.0
Filter width (μm)	0.225	0.29	0.38	0.5
Background (e$^-$/s/pixel)	0.1	0.2	0.6	0.1

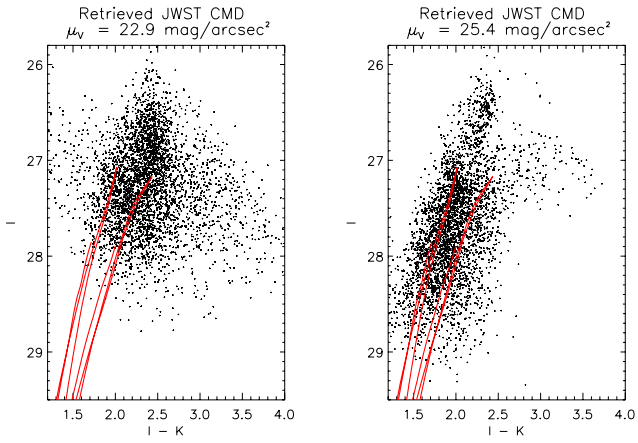

Fig. 16. These are the CMDs obtained from simulations of JWST/NIRCam images, at two different surface brightness, $\mu_V \sim 22.9$ mag/arcsec^2 and 25.5 mag/arcsec^2. The input CMD, and the red isochrones are the same as in Fig. 7. The field of view simulated is 10 times larger than for MICADO/MAORY (reflecting the larger pixel size), and these CMDs come from 7.5 arcsec square images.

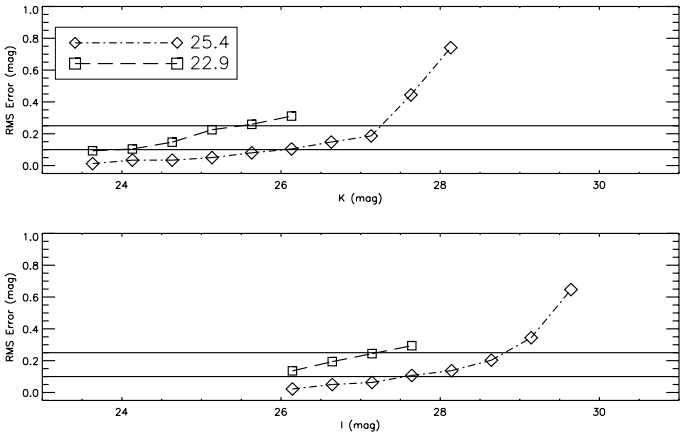

Fig. 17. The photometric errors for JWST/NIRCam images in I and K_s filters, at the maximum surface brightness where photometry can still be achieved ($\mu_v \sim 22.9$ mag/arcsec^2) and also for an uncrowded case ($\mu_v \sim 25.4$ mag/arcsec^2).

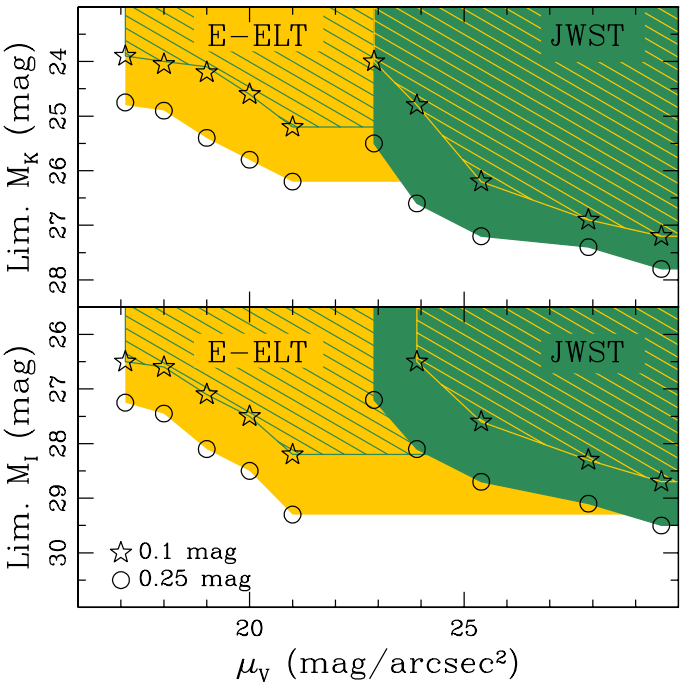

Fig. 18. The surface brightness and limiting magnitude limits are shown for E-ELT (MICADO/MAORY) and JWST (NIRCam) photometry of resolved stars in an old galaxy at the distance of Virgo (17 Mpc). The open star symbols show the sensitivity for photometric errors ±0.1 mag and the open circles for more conservative photometric errors of ±0.25 mag.

5. Interpretation

5.1. Stellar photometry with MCAO images

Ancient resolved stellar populations have up to now been predominantly studied at optical wavelengths. This is because the sensitivity of telescopes and instruments has always been better in the optical, and also old metal-poor stellar populations tend to be relatively blue on the RGB compared to metal rich stellar populations of any age (see Fig. 5). However, there have also been specific cases where the IR is used, for example, regions of high or variable dust extinction. There is presently a move towards IR optimised facilities. This is partly driven by the demands of detecting and studying extremely high red-shift galaxies, but it is also where it is possible to accurately correct for atmospheric effects and reach the diffraction limit for ground-based telescopes. Both JWST and E-ELT are optimised for the IR. For the E-ELT this is determined by the technology limitations of being able to make sufficiently accurate AO corrections.

Here we have presented a very specific technical study of one hypothetical resolved stellar population, in order to assess the feasibility of obtaining accurate photometry with MICADO/MAORY (in I, J, H, K_s filters) for resolved stars in crowded fields at the distance of Virgo. The main advantage that the MICADO/MAORY instrument will have over all others being planned at present, including NIRCam on JWST, is the extremely high spatial resolution it should be capable of at optical/IR wavelengths. This provides a unique opportunity to look at resolved stellar populations deep in the heart of elliptical galaxies (the best examples of which are in the Virgo cluster, at 17 Mpc distance). Thus, the primary aim of this study was to see how well stars could be resolved and photometered in much higher surface brightness (crowded) conditions than are feasible at present. The conclusion is that this is a rather challenging, but viable, aim.

We have shown that despite the very peculiar PSF (see Fig. 1), especially in the I filter, accurate photometry can be carried out even with current standard photometry packages. However, there is certainly room for improvement to optimise photometry algorithms to deal with complex MCAO PSFs, as the photometric errors are still relatively large, even at bright magnitudes. It will also undoubtedly be possible in the future to improve the accuracy of photometry in crowded regions using PSF reconstruction techniques. The better determined are the PSF properties the more precisely it will be possible to remove bright stars from an image and photometer the fainter stars.

We have found that it is possible to reach much fainter magnitude limits in I, in the same exposure time, than in J, H or K_s and the deepest luminosity functions will be obtained in this filter. This is a slightly surprising result given that the AO correction is much less effective in I, compared to J and K_s. This means that not even the much better AO performance, and better defined and more sharply peaked PSFs in the IR filters can compensate for the difference in sky brightness that drives the basic sensitivity difference. For example in the J filter the strehl is a factor ∼3 better than in the I filter (see Table 3). This means that the signal in the central aperture of the PSF is $\sqrt{3}$ better than in I. However, the background in J is 16.5 mag; and in I it is 19.7 mag, which is a difference of ∼3 mag. These effects do not balance out, and so the sky background dominates, with the result that the I filter is significantly more sensitive than J, H or K_s.

It has long been known that the larger is the colour baseline, the more spread out will be the RGB (see Fig. 5). In principle this should make it easier to interpret a CMD more accurately in terms in age and metallicity using $I-K$ colours rather than $J-K$. As Figs. 8 and 10 show, this is not such a clear-cut argument as the sensitivity plots might suggest. Figure 8 shows that strictly speaking $I-K$ is more detailed than $J-K$, but not with a huge significance. Figure 10 shows how clearly the choice of the best filter combinations depends upon the colours of the stars being observed. The redder the stars the larger has to be the difference between the magnitude limit in I and K_s for the sensitivities to be matched. In fact the average $I-K$ colour of the RGB in our simulations, which is probably quite blue for a typical giant elliptical galaxy, ranges between 2 and 3, which matches quite well the sensitivity difference between I and K_s for MICADO/MAORY. If the K_s sensitivity were to increase this would not affect *these* observations. In the case of a much redder stellar population ($I-K > 2.8$), then the strongest limitation on the depth of the CMDs would be the I magnitude (see Fig. 10).

An important question to ask, based on these simulations, is: is the I filter crucial for the science case addressed in this paper? Does it lead to a sufficient improvement in scientific return to warrant the large amount of effort to install it? The answer is not a straight forward yes or not. It is certainly the most sensitive filter for the observations of the bulk of the resolved stellar populations, and especially for metal poor stars. The $I-K$ colour is usually more spread out than $J-K$, and this may often make it easier to disentangle complex stellar populations more accurately in $I-K$, see Fig. 8. However, given the fundamental limits on JHK sensitivity for the specific case of photometering the RGB of old stellar populations in galaxies in Virgo, there is no reason to prefer one filter over the other. However, for CMD analysis we need a colour for the most accurate analysis. Thus at present, for this science case, the answer is that care should be taken that the I filter PSF and sensitivity is delivered

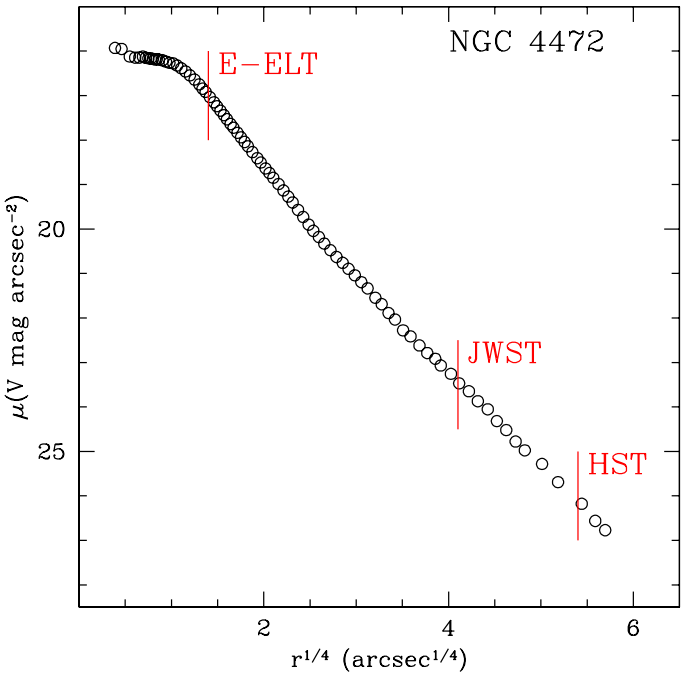

Fig. 19. Here we plot the surface brightness profile of NGC 4472 (from Kormendy et al. 2009), a "typical" giant elliptical galaxy in the Virgo cluster. There is a vertical line placed at the distance from the centre of the galaxy at the highest surface brightness for which CMDs can be made and photometered with E-ELT and JWST (coming from this study), and HST/ACS (Durrell et al. 2007).

as has been presented now. The PSF from MAORY has been provided on a "best effort" basis, and it is at the limits of what is thought to be possible given the current technical specifications of both MAORY and the telescope adaptive mirror (M 4). In conclusion the *I* filter should remain part of the "standard" filter set of any MCAO system for the E-ELT, even with a minimal AO performance.

A possible upgrade path for the telescope may allow better AO performance in the optical which could lead to deep *I* luminosity functions, which can also be used to interpret the properties of distant stellar populations. If the sensitivity of the *I* filter can be pushed to reach the Horizontal Branch limit in Virgo ($I \sim 31$), then it will be possible to directly and unambiguously determine the presence of an ancient and/or metal-poor stellar populations in elliptical galaxies in the Virgo cluster.

A good observing strategy for studying elliptical galaxies will be to use three filters, namely I, J and K_s. The $I-K$ combination will be most useful for studying the metal poor population, or to determine if one is present. The $J-K$ colour will be more revealing about the presence of extremely red evolved stars, such as carbon stars and metal rich AGB stars.

5.2. What we may learn about elliptical galaxies

The centre of a giant elliptical galaxy in Virgo typically has a central surface brightness, $\mu_v \sim 16$ mag/arcsec^2. Our simulations suggest MICADO/MAORY will be able to detect individual stars, even old, metal poor stars, close to the central regions of such a galaxy. It will be possible to make CMDs within 5 arcsec of the centre, of even the largest elliptical galaxies, compared to 250 arcsec for JWST, as is shown in Fig. 19.

Of course, as can be seen from Fig. 7, the amount of information that can be extracted from a CMD at a surface brightness, $\mu_v = 17$ mag/arcsec^2 is likely to minimal. Assuming that the distance to the galaxy is very well known, then it will be possible to tell if we are looking at the AGB star population. If the distance is uncertain, and it is not known a priori if a stellar population contains AGB stars or not, then there will be no clear way of deciding if AGB or RGB stars are being detected from this kind of CMD.

All the CMDs in Fig. 7 are still only of the upper region of the RGB in a Virgo galaxy, so it is not always going to be possible to disentangle the complex star formation histories. However, a much longer exposure time will of course improve the faint limit for accurate photometry. Even though these CMDs of the RGB are not the ideal CMDs to make a unique interpretation (e.g., Gallart et al. 2005), it should also be possible to determine the age and metallicity spread (see Fig. 5). In the case of distinct age or metallicities differences, such as we used for our simulations, it may often be possible to infer their presence.

Well populated CMDs will allow accurate studies of the relative properties within galaxies, and how galaxies may vary compared to each other. This means comparative studies of how the numbers of stars of different colours and luminosity vary with position, and the relative importance of different types of stars on the RGB at different positions. This will provide valuable information as to how the stellar population was built up. It will be interesting to compare the stellar populations in low surface brightness regions (where the photometry is more accurate) with higher surface brightness regions in the same galaxies, or low surface brightness dwarf galaxies with the giants. This will require a detailed understanding of the crowding and incompleteness properties of the CMDs.

It should not be forgotten that the CMDs presented, in Fig. 7 are for extremely small fields of view (0.75 arcsec squared), and when the full field of MICADO is considered 5000 times more stars will be included in each CMD. These cover a range of surface brightness going from the inner to the outer regions of a typical elliptical galaxy. The surface brightness variation is typically very smooth for elliptical galaxies, but for theses types of stars, a global colour and luminosity can hide a lot of variation (e.g., Monachesi et al. 2011). Comparing the resolved stellar populations of the inner and outer regions of elliptical galaxies will have important implications for formation scenarios.

For these kinds of relative studies a large field view (compared to the size of the galaxy being studied) is required. The major advantage of an MCAO imager for this science case, is the wide field of view that is possible (~53 arcsec square), with uniform AO correction. This allows an accurate and detailed comparative study of a significant area of most elliptical galaxies at the distance of Virgo.

Figure 20 shows, from the surface brightness limits of MICADO/MAORY imaging, how many galaxies in Virgo (from Kormendy et al. 2009) can be studied in detail, to which distance from the centre, in a one hour exposure. We can see that it will be possible to resolve the entire stellar population of dwarf spheroidal galaxies, as they are uniformly low surface brightness systems. It should be realised that most of the central regions of galaxies in Virgo are no more than 1−3 arcmin across, at a surface brightness of ~22 mag/arcsec^2. The wide field of MICADO/MAORY will thus efficiently allow the sampling of a range of surface brightness across each galaxy.

Of course MICADO/MAORY will also be able to make more detailed CMDs of closer by giant elliptical galaxies, such as NGC 3379 (M 105) the dominant member of the Leo group, at a distance of 10.5 Mpc (Salaris & Cassisi 1998). This is thus 0.7 mag closer than the simulations at the distance of Virgo

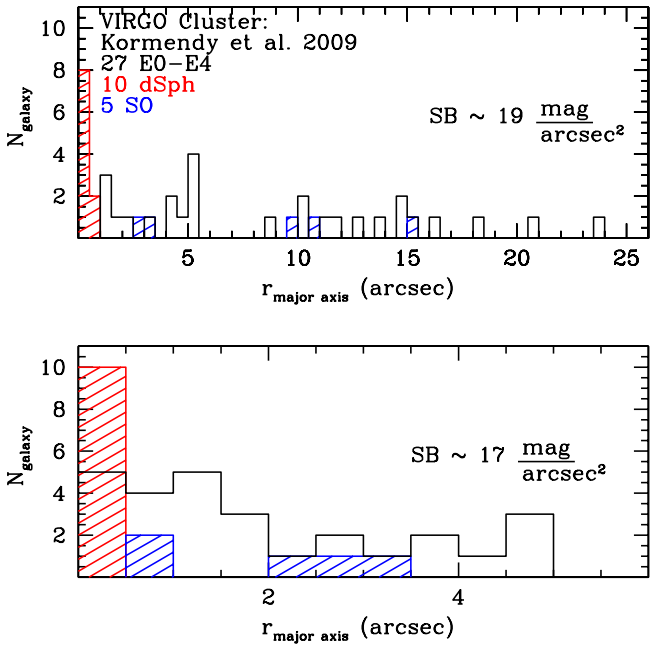

Fig. 20. For a sample of galaxies in the Virgo cluster (taken from Kormendy et al. 2009) we plot the position on the major axis (in arcsec) to which they can be resolved into individual stars using MICADO/MAORY at two different surface brightness limits (SB). The same sample of galaxies is plotted in each case; 10 dwarf spheroidals (in red); 27 elliptical galaxies (black) and 5 S0 galaxies (blue).

shown here. This means that the CMDs will go 0.7 mag deeper in each filter for the same photometric errors, at the same surface brightness. The central surface brightness of NGC 3379 is about $\mu_V = 19$ mag/arcsec^2. So we can look in the centre of this galaxy and go 0.7 mag deeper than the 19 mag/arcsec^2 (and fainter surface brightness) CMDs shown in Fig. 7 in one hour of integration time.

6. Conclusions

In this paper we have carefully simulated images which can be expected for MICADO/MAORY on a 42-m E-ELT, of an old resolved stellar population at the distance of Virgo in four broad band filters (I, J, H, and K_s). These simulations are based upon the most detailed information about the telescope and instrument characteristics currently available. We restricted ourselves to one narrowly defined science case, for one stellar population. Keeping this aspect of the study fixed allowed us to restrict the number of variables that had to be considered, which leads to a clearer understanding of the the importance of observational and instrumental effects, such as sky brightness, seeing, Strehl and PSF. There is certainly scope for expanding this study to other types of stellar populations, especially those at closer distances where it will be possible to make accurate CMDs of the main sequence turnoff region.

For our science case we found that reaching the tip of the RGB at the distance of Virgo is clearly feasible in two filters in observations of one hour per filter, when the surface brightness is no higher than 17 mag/arcsec^2. Deeper CMDs, in the same exposure time, are possible for a surface brightness of less than 20 mag/arcsec^2, where CMDs can reach ~2 mags below the tip of the RGB. Thus, our simulations suggest that obtaining accurate CMDs for resolved stellar populations in elliptical galaxies at the distance of the Virgo cluster is a challenging goal, but feasible, especially when exposures times longer than one hour are considered.

We suggest that the best strategy for resolving and photometering individual old stars at the distance of Virgo is to use three filters, namely I, J and K_s. The $I-K$ combination will be most useful for studying the metal poor population, or to determine if one is present. The $J-K$ colour will be more revealing about the presence of extremely red evolved stars, such as carbon stars and metal rich AGB stars.

We also performed simulations in a similar fashion for the NIRCam imager on JWST. This will clearly work at a different (barely overlapping) surface brightness range to MICADO/MAORY. Of course the wider field of view and larger pixels of NIRCam are better suited for studying the properties of the extended halos of galaxies. From this comparison we can infer that MICADO/MAORY and NIRCam will be a useful complementary pair for detailed studies of giant elliptical-like galaxies in Virgo. MICADO/MAORY will be able to probe the high density central parts, and NIRCam will be more effective at observing the extensive outer regions. Thus the two instruments will allow us to study large and small scale properties of the resolved stellar populations in a large number of elliptical galaxies of all sizes and characteristics in Virgo.

Acknowledgements. This paper grew out of discussions during the E-ELT MICADO phase A study, and was expanded after the completion of the MAORY Phase A study. We thank Enrico Marchetti for useful discussions and comments on an early version of this manuscript. We thank Renato Falomo for interesting discussions during the MICADO Phase A study. We are grateful for funding for this project from an NWO-VICI grant (A.D., G.F. and E.T.), as well as ESO funding for MICADO and MAORY phase A studies.

References

Aparicio, A., & Gallart, C. 2004, AJ, 128, 1465
Binggeli, B., Sandage, A., & Tammann, G. A. 1985, AJ, 90, 1681
Bono, G., Calamida, A., Corsi, C. E., et al. 2009, in Science with the VLT in the ELT Era, ed. A. Moorwood, 67
Caldwell, N. 2006, ApJ, 651, 822
Campbell, M. A., Evans, C. J., Mackey, A. D., et al. 2010, MNRAS, 405, 421
Capaccioli, M., Vietri, M., Held, E. V., & Lorenz, H. 1991, ApJ, 371, 535
Castelli, F., & Cacciari, C. 2001, A&A, 380, 630
Clénet, Y., Bernardi, P., Chapron, F., et al. 2010, SPIE, 77363Q
Condon, J. J. 1974, ApJ, 188, 279
Cox, C., & Hodge, P. 2006, SPIE Conf. Ser., 6265
Davies, R., & Genzel, R. 2010, The Messenger, 140, 32
Davies, R., Ageorges, N., Barl, L., et al. 2010, SPIE, 77352A
Diolaiti, E. 2010, The Messenger, 140, 28
Diolaiti, E., Bendinelli, O., Bonaccini, D., et al. 2000, SPIE Con. Ser., 4007, ed. P. L. Wizinowich, 879
Durrell, P. R., Williams, B. F., Ciardullo, R., et al. 2007, ApJ, 656, 746
Falomo, R., Pian, E., Treves, A., et al. 2009, A&A, 501, 907
Ferraro, F. R., Dalessandro, E., Mucciarelli, A., et al. 2009, Nature, 462, 483
Fiorentino, G., Tolstoy, E., Diolaiti, E., et al. 2010, A&A, submitted
Foppiani, I., Diolaiti, E., Lombini, M., et al. 2010, in Adaptative Optics for Extremely Large Telescopes
Gallart, C., Aparicio, A., & Vilchez, J. M. 1996, AJ, 112, 1928
Gallart, C., Zoccali, M., & Aparicio, A. 2005, ARA&A, 43, 387
Gilmozzi, R., & Spyromilio, J. 2007, The Messenger, 127, 11
Hook, I., & The Opticon ELT Science Working Group 2007, Overview of the Science Case for a 50 100 m Extremely Large Telescope (Springer Verlag), 121
Johns, M. 2008, SPIE Conf. Ser., 6986
Jolissaint, L., Véran, J., & Conan, R. 2006, J. Opt. Soc. Amer. A, 23, 382
Kissler-Patig, M., Lyubenova, M., & ESO ELT Science Working Group 2009, An Expanded View of the Universe – Science with the European Extremely Large Telescope (ESO), 56
Kormendy, J., Fisher, D. B., Cornell, M. E., & Bender, R. 2009, ApJS, 182, 216
Maraston, C., Daddi, E., Renzini, A., et al. 2006, ApJ, 652, 85
Marchetti, E., Brast, R., Delabre, B., et al. 2006, SPIE Conf. Ser., 6272

Momany, Y., Ortolani, S., Bonatto, C., Bica, E., & Barbuy, B. 2008, MNRAS, 391, 1650
Monachesi, A., Trager, S. C., Lauer, T. R., et al. 2011, ApJ, 727, 55
Moretti, A., Piotto, G., Arcidiacono, C., et al. 2009, A&A, 493, 539
Najita, J., The, & Science Working Group 2002, Enabling a Giant Segmented Mirror Telescope for the astronomical community (Washington: AURA)
Olsen, K. A. G., Blum, R. D., & Rigaut, F. 2003, AJ, 126, 452
Origlia, L., Lena, S., Diolaiti, E., et al. 2008, ApJ, 687, L79
Pietrinferni, A., Cassisi, S., Salaris, M., & Castelli, F. 2004, ApJ, 612, 168
Renzini, A. 1998, AJ, 115, 2459
Rieke, M. J., Kelly, D., & Horner, S. 2005, SPIE Conf. Ser., 5904, ed. J. B. Heaney, & L. G. Burriesci, 1
Salaris, M., & Cassisi, S. 1998, MNRAS, 298, 166
Sana, H., Momany, Y., Gieles, M., et al. 2010, A&A, 515, A26
Schechter, P. L., Mateo, M., & Saha, A. 1993, PASP, 105, 1342
Scheuer, P. A. G. 1957, in Proc. Cambridge Phil. Soc., 53, 764
Silva, D., Hickson, P., Steidel, C., & Bolte, M. 2007, TMT Detailed Science Case: 2007 TMT Document Number: TMT.PSC.TEC.07.003.REL01, 87
Sollima, A., Ferraro, F. R., Origlia, L., Pancino, E., & Bellazzini, M. 2004, A&A, 420, 173
Spyromilio, J., Comerón, F., D'Odorico, S., Kissler-Patig, M., & Gilmozzi, R. 2008, The Messenger, 133, 2
Stephens, A. W., Frogel, J. A., DePoy, D. L., et al. 2003, AJ, 125, 2473
Stetson, P. B. 1987, PASP, 99, 191
Szeto, K., Roberts, S., Gedig, M., et al. 2008, SPIE Conf. Ser., 7012
Tolstoy, E. 2010 [arXiv:1012.2229]
Tolstoy, E., Hill, V., & Tosi, M. 2009, ARA&A, 47, 371
Tolstoy, E., Battaglia, G., Beck, R., et al. 2010 [arXiv:1009.4103]
Wyse, R., & the Stellar Populations Working Group 2002, Enabling a Giant Segmented Mirror Telescope for the astronomical community (Washington: AURA), Appendix 2C
Yi, S., Demarque, P., Kim, Y., et al. 2001, ApJS, 136, 417